UNIVERSITY OF KWAZULU-NATAL

PERFORMANCE EVALUATION OF FSO COMMUNICATION SYSTEMS OVER WEAK ATMOSPHERIC TURBULENCE CHANNEL FOR EASTERN COAST OF SOUTH AFRICA

Henry Ogunmodede

Supervised by:

Professor Thomas J.O. Afullo

Dr. Pius A. Owolawi

2017

PERFORMANCE EVALUATION OF FSO COMMUNICATION SYSTEMS OVER WEAK ATMOSPHERIC TURBULENCE CHANNEL FOR EASTERN COAST OF SOUTH AFRICA

Henry Ogunmodede

Supervised by:

Professor Thomas J.O. Afullo

Dr. Pius A. Owolawi

Submitted in fulfilment of the academic requirements for the degree of Master of Science in Engineering.

College of Agriculture, Engineering and Science, University of KwaZulu-Natal, Durban, South Africa

June 2017

As the candidate's supervisor I agree to the submission of this dissertation.

Date of Submission: _____

Supervisor: _____

Professor Thomas J.O. Afullo

Dedication

To my family, and in loving memory of my dad, Banji Ogunmodede

Acknowledgements

I would like to express my profound gratitude to my supervisor Professor Thomas J.O. Afullo, for his support, advice, invaluable guidance and persistent encouragement throughout this research work. I would also like to thank him for proof reading this dissertation and for giving me the privilege to undertake my studies within his research group. I am especially grateful to him for his understanding and fatherly support during my hard times in the course of my research.

Declaration

I, Henry Ogunmodede, declare that,

i. The research reported in this dissertation, except where otherwise indicated, is my original work.
ii. This dissertation has not been submitted for any degree or examination at any other university.
iii. This dissertation does not contain other persons' data, pictures, graphs or other information, unless specifically acknowledged as being sourced from other persons.
iv. This dissertation does not contain other persons' writing, unless specifically acknowledged as being sourced from other researchers. Where other written sources have been quoted, then:
    a. Their words have been re-written but the general information attributed to them has been referenced;
    b. Where their exact words have been used, their writing has been placed inside quotation marks, and referenced.
v. Where I have reproduced a publication of which I am an author, co-author or editor, I have indicated in detail which part of the publication was actually written by myself alone and have fully referenced such publications.
vi. This dissertation does not contain text, graphics or tables copied and pasted from the Internet, unless specifically acknowledged, and the source being detailed in the dissertation and in the References sections.

Signed: _____

Abstract

Free space optical (FSO) communication, otherwise known as optical wireless communication (OWC), is an established line-of-sight telecommunication technique which utilises an optical signal carrier to propagate modulated signals in the form of a light wave (visible or infrared) over the atmospheric medium. It has numerous advantages, including ease of deployment, large bandwidth, cost effective, full duplex high data rate throughput, protocol independence, highly secured data rate transmission, unregulated frequency spectrum, limited electromagnetic interference, and minimum amount of power consumption.

With all the inherent advantages in FSO systems, the technology is impaired by atmospheric turbulence. Atmospheric turbulence occurs due to the persistent random changes of the refractive index as a result of variations in atmospheric temperature and pressure. This results in fluctuations in the irradiance of the laser (simply referred to as scintillation), which may lead to attenuation of optical signals in the FSO communication system. Thus, atmospheric attenuation and turbulent conditions have negative effects on the performance and ease of deployment of FSO communication systems. In this dissertation, we examine the performance of FSO systems over weak atmospheric turbulence channel for the eastern coast of South Africa.

We evaluate the feasibility of the FSO link and how to improve the reliability by estimating the link margin, probability of attenuation exceedance, power scintillation index, overall power loss due to attenuation and turbulence, link budget estimate for different link lengths and wavelengths. The FSO system availability estimated for the eastern coast of South Africa is above 99% for link distances ranging from 1 km-4 km at 850 nm, 950 nm and 1550 nm. It is also observed that the FSO link availability increases with corresponding increase in wavelengths.

Adopting the Kim model to estimate the atmospheric attenuation at 850 nm wavelength, the attenuation due to scattering contributes 9.47% to the absolute atmospheric losses while the atmospheric turbulence loss contributes 90.53% to the overall power loss at a link range of 4 km. Using the Ferdinandov model for a link range of 4 km at 950 nm wavelength, the attenuation due to scattering contributes 8.81% to the total power loss while the atmospheric turbulence loss contributes 91.19% to the overall power loss.

It is observed that the attainable link distance increases with increase in atmospheric visibility status. The FSO system availability reduces with increase in the propagation link distance. Furthermore, it is found that the fading loss from scintillation effects strongly depends on the power scintillation index. An increase in the power scintillation index, causes an increase in the fading loss. Thus, the power scintillation index also increases per unit increase in transmission link length and refractive index.

The compensation margin for such atmospheric fading loss increases with decrease in accessible FSO system bound probability. Therefore, for a highly reliable FSO system link, extra margin must be incorporated to compensate for fading loss caused by scintillation.

Table of Contents

List of Figures

List of Tables

Glossary of Abbreviations

3G	Third generation
4G	Fourth generation
ANSI	American National Standards Institute
APD	Avalanche photo-detector
AWGN	Additive white Gaussian noise
BER	Bit error rate
bps	Bits per second
BPSK	Binary phase shift keying
CDMA	Code division multiple access
CDRH	Center for Devices and Radiological Health
CENELEC	European Committee for electrotechnical Standardization
CF	Carrier frequency
CO_2	Carbon dioxide
CW	Continuous wave
DC	Direct current
DPSK	Differential phase shift keying
DSL	Digital subscriber loop
FOV	Field of view
FPGA	Field-programmable gate array
FSO	Free space optics
FTTH	Fibre to the home
HTTP	Hypertext Transfer Protocol
GaAs	Gallium arsenide
Gbps	Giga bit per second
Ge	Germanium
HDTV	High definition television
He-Ne	Helium-Neon
H-V	Hufnagel-Valley model of index of refraction structure parameter
HO	Host Oscillator
IEC	International electrochemical commission
IM/DD	Intensity modulation/direct detection
IR	Infra-red
ISI	Inter symbol interference

LAN	Local area network
LDPC	Low density parity codes
LED	Light emitting diode
LIA	Laser Institute of America
LOS	Line of sight
MIMO	Multiple-input multiple output
MLCD	Mars Laser Communication Demonstration
NASA	National Aeronautics and Space Administration
NEC	Nippon Electric Company
OBPF	Optical band pass filter
OFDM	Orthogonal frequency division multiplexing
OWC	Optical wireless communication
OOK	On-off keying
PAT	Pointing, acquisition and tracking
PD	Photodiode
Pdf	Probability density function
PIN	p-type-intrinsic-n-type photo-detector
P_{out}	Outage probability
PSD	Power spectral density
QAM	Quadrature amplitude modulation
QPSK	Quadrature phase shift keying
RF	Radio frequency
RoFSO	Radio over free space optics
S.I.	Scintillation Index
SILEX	Semiconductor Laser Inter-satellite Link Experiment
SNMP	Simple Network Management Protocol
SNR	Signal to noise ratio
THz	Terahertz
TT	Transmitter telescope
TV	Television
UWB	Ultra wide band
WDM	Wavelength division multiplexing
WOCS	Wireless optical communication system

Glossary of Symbols

A_d	Aperture diameter of the receiver
λ	Carrier wavelength
$(4\pi/\emptyset^2)_{dev(op)}$	Optical beam deviation
$(4\pi/\emptyset^2)_{dev(RF)}$	RF beam deviation
L	Link length
$\tau(\lambda, L)$	Transmittance of the atmospheric channel
P_{tx}	Power emitted from transmitter
P_{rx}	Power received at a transmission link length *L*
$\gamma_{tx}(\lambda)$	Attenuation/fading coefficient (m^{-1})
$\alpha_a(\lambda)$	Aerosol absorption coefficients
$\alpha_m(\lambda)$	Molecular absorption coefficients
$\beta_a(\lambda)$	Aerosol scattering coefficient
$\beta_m(\lambda)$	Molecular scattering coefficients
m_0	Size parameter
r	Particle radius
Q_e	Mie scattering efficiency
$\grave{n}$	Real part of the complex index of refraction
$n(r)$	Fog molecules per unit volume
ϵ	Optical threshold
$V(km)$	Visibility values in kilometres
λ_0	Visibility rang reference wavelength
A_{att}	Atmospheric attenuation
q	Molecule size distribution
${C_R}^2$	Refractive index in $(m^{-2/3})$
wp	Wind speed in (ms^{-1})
a	Altitude in (m)
T_I	Turbulence intensity on the ground
k	Optical wave number in (m^{-2})

S_I	Scintillation Index
S_{att}	Scintillation attenuation
x	Propagating optical signal
$erfc$	Error complementary function
${s_d}^2$	Standard deviation of Log normal distribution
μ_x	Mean of the Log normal (Pdf)
$P(X)$	Log Normal distribution (Pdf)
P_{scin}	Power scintillation Index
F_m	Required compensation margin for losses due to scintillation in the atmosphere.
d_R	Receiver diameter
d_T	Transmitter diameter
A_D	Aperture area of the receiver
A_{Tx}	Aperture of the Transmitter
A_s	Laser Source
G_{loss}	Geometric loss in $[dB]$
θ_s	Divergence angle of the optical source
M_L	Link Margin
P_m	Optical laser Power in $[dB]$
A_T	Transmitter coupling loss
θ	Beam Divergence Angle
A_R	Receiver coupling loss
P_{rs}	Receiver Sensitivity in $[dBm]$
D_A	Aperture Diameter
M_0	FSO system parameter constant
$A_{att}(L)^*$	Overall atmospheric losses

V_{min}	Required minimum visibility
L_{avail}	Link availability
F_C	Cumulative distribution function

Chapter 1 - Introduction

1.1 Background of FSO

About 800 BC, fire beacons were employed by the earliest Romans and Greeks to make signs for communication, likewise in 150 BC, smoke waves were used by the American Indians for communication purpose as well. Various methods for visible signaling were utilized. In the year 1790, Claude Chappe of France employed electronic devices to effect free space optical systems by introducing the optical telegraph and the French ocean sailors used Semaphore for optical signaling. In the year 1880, Alexander Graham Bell exhibited what was referred to as the first ever free space optical communication over a wireless medium. He introduced a device called a "Photo phone". This device transforms audible tones into electrical radio tones which are propagated over a certain range utilizing modulated sunlight as a carrier signal. However, the performance of the system was poor due to the roughness of the device materials adopted as well as the random behaviour of sunlight [1].

In 1960, FSO started gaining momentum with the invention of Laser technology at Hughes Research Laboratories, Malibu, California, USA [2]. Numerous FSO experiments were carried out in military Laboratories between the early 1960s and the 1970s. In 1962, a group of researchers at the Massachusetts Institute of Technology (MIT) Lincoln Laboratory employed a GaAs LED for a remarkable propagation of radio signals through a distance of approximately (48km); while in May 1963, in between Panamint Ridge and San Gabriel Mountain, USA at approximately (190km), a modulated voice signal was propagated using a Helium-Neon (He-Ne) laser. In March 1963, some sets of researchers at the North-America Aviation carried out the first TV-over-Laser experiment. Later in 1970, Nippon Electric Company (NEC) in Japan invented the first ever full duplex (He-Ne) laser with 0.6328 capacity for FSO medium over a distance of approximately 14 km between Yokohama and Tamagawa [3].

Afterwards, the military has consistently researched and mainly employed FSO technology for private intercommunications. NASA and ESA use programmes like the Mars Laser Communication Demonstration (MLCD) as well as the Semiconductor Laser Inter-satellite Link Experiment (SILEX) to extensively research the FSO technology for deep space applications [4]. In the1990s, verging on the fast development and advancement of optical electronic technologies, the FSO technology had now experienced a rebirth. Moreover, the enormous demand for larger bandwidth and high capacity access networks, due to the emergence of the internet, has reawakened the use of FSO. The fiber-optic technology was well-established, and numerous researchers had discovered diverse means to apply these effective, low-cost materials in FSO networks. Various technological advancements have supported this development such as the advent of

erbium-doped fibre amplifiers, wavelength-division-multiplexing (WDM) as well as photodiodes and photodetectors which have the capabilities to perform efficiently at greater wavelengths [5].

Additionally, the continuing call for higher bandwidth in the presence of modern and reigning applications shows that the aged tradition of depending on a single access network to link with the ultimate users must be prevented. These factors combined with the noted achievements of its use in military operations have renewed the interest in its civil applications between access systems [6, 7]. Numerous successful field experiments have been documented in the past few years at different parts of the globe which have further motivated investment in FSO [8, 9]. This has now developed into the massed commercialization and installation of FSO in the present day's telecommunication framework.

Presently, the physical layer FSO technology is considered as a backup scheme in solving current communication problems, generally the demand by the end users is access to immense data rate at economic costs [10, 11]. The hybridization of the FSO system with existing access technologies is far more rapid because it is visible to the data protocol and the traffic type. Nonetheless, the main challenges such as the FSO atmospheric fading and the atmospheric turbulence as well as achieving 99.999% link availability, still need to be overcome in order to increase the FSO link length and link availability in physical layer FSO systems [12, 13].

1.2 Research Motivation

Over the years, there has been an enormous increase and development of telecommunication and electronic devices such as iPads, iPods, cameras, smart phones, laptops, television, printers, oven etc. These give rise to the use of various data consuming applications like skype, periscope, YouTube mobile app, hangout, WhatsApp, IMO and so on to perform activities like live-chat, video-chat, live coverage/streaming etc. which result in immense and intense demand for high bandwidth demanding high capacity access network. This consistent and continual requirement for more bandwidth has resulted in exhaustion of the traditionally employed fibre optics radio frequency (RF) spectrum. This optical fibre technology has various drawbacks like overcrowded frequency spectrum, high license fees, unsecure low data streams, difficulty in deployment, immobile, the high cost of deployment, minimum coverage service in certain local areas etc. In view of the aforementioned shortcomings in the optical fibre communication systems; an alternative high capacity access communication system is required. Wireless optical communication system (WOCS) is now gaining momentum among researchers as a viable solution for high/immense capacity network accessibility due to its various advantages such as high bandwidth, low power consumption, license-free frequency spectrum, simple and low cost of installation, small size etc. over its optical fibre communication system counterpart.

1.3 Research Objectives

This dissertation is mainly aimed at evaluating the performance of FSO communication systems over weak atmospheric turbulence channel for the eastern coast of South Africa. Additionally, it also aimed to find techniques to mitigate the effect of atmospheric turbulence on the performance of FSO communication systems. Specific research objectives has been summarized in order to achieve these aims:

- To examine the fundamental theory of a physical layer FSO technology and the challenges imposed on the FSO communication system performance.
- To examine the features of the FSO weak atmospheric channel, and understand the limitations and range of validity of individual model for characterizing the FSO channel attenuation caused by atmospheric turbulence.
- To carry out a feasibility study of FSO communication systems for the eastern coast of South Africa using atmospheric visibility data such as (rain, fog, wind speed, sunshine, humidity, temperature, wind direction, pressure etc.). These statistical data will be analyzed to determine the performance of FSO communication system for the eastern coast of South Africa.
- To determine minimum, average and maximum visibility values and wind speed for the eastern coast of South Africa. Minimum, average and maximum atmospheric attenuation due to various atmospheric scattering modelled with (Kim, Kruse, Ferdinandov etc.) will be estimated for the eastern coast of South Africa using the visibility data.
- To determine turbulence losses and carry out an analysis of the contribution of scattering and turbulence towards atmospheric loss in FSO communication system will also be examined.
- To carryout link budget analysis and examine the link availability of FSO systems for the eastern coast of South Africa.
- To determine the performance of physical layer FSO systems based on M-DPSK, M-QAM and BPSK in a turbulent atmospheric channel.

1.4 Research Contributions

In the course of the research, the author has:

- Evaluated the feasibility of the FSO link for the eastern coast of South Africa using atmospheric visibility data such as (rain, fog, wind speed, sunshine, humidity, temperature, wind direction, pressure etc.).
- Estimated the atmospheric attenuation due to various atmospheric scattering modelled with (Kim, Kruse, Ferdinandov etc.) for the eastern coast of South Africa using visibility data.

- Estimated the probability of attenuation exceedance, power scintillation index and overall power loss due to attenuation and turbulence.
- Determined the link budget and link availability of FSO systems for the eastern coast of South Africa.
- Investigated the performance of OFDM systems mitigated by M-DPSK over FSO channel, in non-turbulence and turbulence environment. Also, evaluated the performance of OFDM-FSO communication system under Log-normal channel for MQAM and BPSK modulation schemes.

1.5 Thesis Structure

This dissertation comprises of six chapters overall, which are summarized underneath:

Chapter One – Introduction: The background of FSO systems is presented. It also comprises of the specific aims and objectives of the research.

Chapter Two – Fundamentals of FSO: It presents the overview of free space optical communication systems. Also, the advantages and limitations of FSO compared to RF are examined. The features, applications, system configuration and eye safety issues of FSO are examined and discussed.

Chapter Three – Methodological Approach: Examines and discusses the various statistical models used in this dissertation. The Kruse, Kim and Ferdinandov models were adopted to quantify the scattering atmospheric attenuation for the eastern coast of South Africa. The FSO system power scintillation index, optical beam divergence loss, link margin and link availability are discussed as well.

Chapter Four – Results and Discussions: The visibility patterns, from which the atmospheric attenuation coefficients of physical layer FSO systems were determined and analyzed for the eastern coast of South Africa. Effects of power loss due to scattering and scintillation are evaluated. The link margin to compensate for losses caused by scintillation impacts are discussed. The probability of encountering and exceeding atmospheric attenuation is investigated. The FSO link budget and link availability are determined and analyzed.

Chapter Five - Applications: The performance of terrestrial FSO based on M-DPSK, M-QAM and BPSK in a turbulent atmospheric channel is examined and discussed.

Chapter Six – Conclusions and Future Work: Lastly, the summary of major findings is presented in this chapter. The conclusion and the future work is highlighted.

1.6 List of Publications

H. A. Ogunmodede, P. A. Owolawi and T. J. Afullo **"**Performance Analysis of OFDM-FSO Communication Systems Using M-DPSK Modulation" IEEE Optical Interconnects Conference, San Diego, California USA, 9-11 May, 2016.

H. A. Ogunmodede, T. J. Afullo and P. A. Owolawi **"**Performance Evaluation of OFDM-FSO Communication Systems Using MQAM and BPSK Modulation under Log-Normal Channel" Accepted by SATNAC Conference, Fancourt, George, Western Cape, South Africa, 4-7 September, 2016.

Chapter 2 – Fundamentals of FSO

2.1 Introduction

This chapter presents a brief review of the WOCS system, which is significant in comprehending the research work carried out. The theory of FSO communication system, like its areas of application, characteristics, and terminology has been examined. The various optical photo-detection processes are defined. With reference to atmospheric medium, atmospheric fading and scintillation are also highlighted. The chapter concludes with a discussion of the eye safety issues and standards.

2.2 Overview of FSO

WOCS is the communication system that employs optical carriers to propagate data streams over an unguided medium which might be free space or the atmosphere [14]. The wireless optical communication system may be grouped into two major sections, that is indoor and outdoor WOCS. The indoor WOCS utilizes near infra-red (IR) for the exchange of information inside a building where the tendency of installing optical fiber cables is burdensome [15]. Indoor WOCS is divided into four system frameworks namely direct line-of-sight (LOS), non-direct LOS, diffused as well as tracked. The outdoor WOCS also referred to as free space optics (FSO) is further categorized into terrestrial and space links which comprise of house-to-house, ground station-to-satellite, satellite-to-ground station, satellite-to-satellite mediums etc. [16, 17]. Figure 2-1 below illustrates the classification of WOCS.

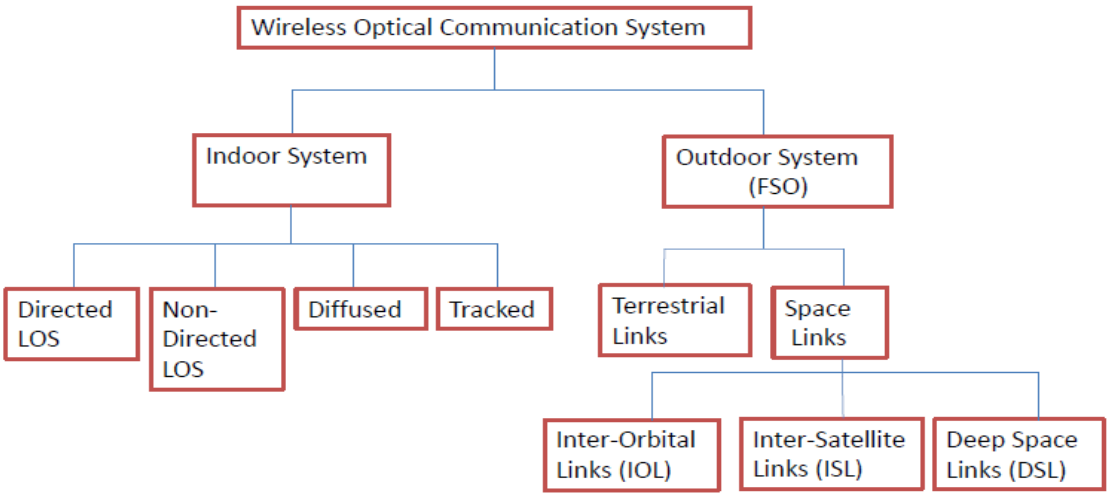

Figure 2-1: Classification of wireless optical communication systems

FSO communication system otherwise known as Wireless optical communication system (WOCS) is a dated line-of-sight telecommunication system which utilizes an optical signal carrier to propagate modulated signals in the form of a light wave (i.e. visible or infrared) over the atmospheric medium [18, 19]. It has numerous advantages such as the ease of deployment, large bandwidth, cost effective, full duplex high data rate throughput, protocol independence, highly secured data rate transmission, unregulated frequency spectrum, limited electromagnetic interference and minimum amount of power consumption [20]. The fundamental theory of FSO propagation is related to optical fiber communication system except that FSO modulated signals are propagated over a random medium in place of guided fiber optic cables.

2.3 Comparison of FSO with RF

FSO technology has a few favourable qualities against its RF counterpart. The significant distinction between FSO and RF communication systems arises from the substantial distinction in their wavelengths. For FSO systems, under clear climate conditions (Visibility is greater than 10 miles), the atmospheric propagation gap falls within the near infrared wavelength spectrum from 700 nm to 1600 nm. The propagation link for RF technology falls within 30 mm to 3 m. Evidently, the RF wavelength is far greater in relation to the optical wavelength. This large disparity of wavelengths prompts for numerous fascinating contrasts between the two technologies as provided below:

I. High Modulation Bandwidth: It is a strongly established fact that a high rise in carrier frequency gives an increase in the data conveying capability of a communication network. The RF as well as microwave communication technologies have about 20% available bandwidth of the carrier frequency (CF). For optical communication, regardless of the bandwidth (assuming 1% of CF at $\approx 10^{16}$), the available bandwidth gives 100 THz. This enables the accessible bandwidth in the order of THz for optical frequency to be very nearly 10^5 times that of the traditional RF carrier systems [21].

II. Narrow beam Deviation: The beam deviation corresponds to $\left(\frac{\lambda}{A_d}\right)$, where A_d represents the aperture diameter while λ denotes the carrier wavelength. Hence, the optical carrier beam dispersion is smaller compared to the RF carrier. This results in an improved signal strength at the receiver for a specific propagated power [22].

III. Low power and mass demand: Considering a specific transmitter power scale, the optical strength is higher at the receiving end as a result of its smaller beam deviation. Hence, the smaller wavelength of the optical carrier allows FSO designers to invent a technology with a smaller antenna compared to that of an RF system to attain the same gain (i.e. antenna gain rate is reciprocal

to the square of the operational wavelength). The conventional range is 0. 3 m versus 1. 5 m for the FSO antenna [23].

IV. High directivity: Due to the fact that optical wavelength is very low, a tremendous directivity is acquired with small-sized FSO antennas. The antenna directivity is nearly equal to its gain. Equation 2.1, shows the ratio of antenna directivity of optical carrier to that of its RF carrier counterpart.

$$\frac{G_{op}}{G_{RF}} = \frac{(4\pi/\emptyset^2)_{dev(op)}}{(4\pi/\emptyset^2)_{dev(RF)}}, \tag{2.1}$$

Where $(4\pi/\emptyset^2)_{dev(op)}$ and $(4\pi/\emptyset^2)_{dev(RF)}$ represents optical and RF beam deviation appropriately and are equivalent to $\left(\frac{\lambda}{A_d}\right)$.

V. License-free frequency spectrum: In RF technology, the main challenge is the adjacent carrier interference which occurs due to frequency spectrum overcrowding. Therefore, the need for spectrum licensing regulatory agencies is required. However, Optical technology spectrum is not licensed to date [24].

VI. Highly Secured: In FSO technology, signals can't be detected with spectrum analyzers or RF measuring devices since FSO lasers are highly directional with extremely small beam deviation [25]. Thus, it is not easily interfered with. Contrary to RF signals, FSO beams cannot go through opaque materials [26].

VII. Simple and Low-cost of installation: The advancement of FSO systems has seen them become less expensive compared to RF systems with identical information streams. No extra expense is incurred for FSO system to provide a proportionate data rate compared to optical fiber [11]. FSO systems are also simple and makes for easy and speedy installation. As such, little time and effort are required to re-install the FSO technology anywhere else with a wide area of coverage [27].

VIII. Weather conditions dependency: The terrestrial FSO system performance is influenced by the state of the atmosphere. The random nature of the atmospheric conditions poses a great challenge on FSO link design. However, it is also notable that both RF and satellite communication channels under heavy rainfall and stormy weather conditions experience channel fading as well.

In addition to the aforementioned advantages, FSO systems provide secondary benefits which include:

- Low power consumption
- It is immune to electromagnetic interference

- Compared to RF, FSO is a non-fixable improvable technology
- The laser radiation should be within a recommended safety range

2.4 Applications of FSO

Listed below are numerous conventional areas where FSO systems may be utilized effectively:

I. Last mile connectivity: The bandwidth gap that is present between the ultimate users and the optical fiber might be connected by employing the FSO system. In present-day markets, technological access with network ranges from 50 m to a couple of kilometers with information streams ranging from 1 Mbps up to 10 Gbps [28].

II. Fiber optics backup network: It is employed to serve as a support/alternative during signal loss or network failure due to damage or poor fiber optics channel conditions. The channel length may be nearly 10 km with information streams of about 10 Gbps [29].

III. Cellular communication system backhaul: It can also be utilized in the third/fourth generation (3G/4G) technology to relief congestion in between ground stations and switching centers, and also to carry IS-95 CDMA information from macro and micro cells locations to the ground stations [29].

IV. Disaster recovery/temporary channels: It can also be applied where a temporary network access is required such as a seminar, conference, workshop or ad hoc accessibility to replace a collapsed existing communication system [30].

V. Multi-college communication system: FSO may also be used to link various college networks together and serve as backup access for Fast-Ethernet as well as gigabit-Ethernet speeds [30].

VI. Difficult terrain: FSO is a viable signal link in situations like over rivers connection, always busy lane, rail paths.

VII. High definition Television: Due to the enormous bandwidth demand of high definition (HD) electronic devices like cameras, laptops, and TV signals, FSO continues to be utilized in the broadcast industry to deliver live information from (HD) cameras from rural areas to city office.

2.5 FSO System Configuration

The system configuration of an FSO network is depicted in Fig. 2-2, it basically comprises of three main parts; namely, transmitter, atmospheric channel and receiver. Each of these parts such optical source, Pin-diode (PIN)/avalanche photo-diode (APD) etc. are further discussed in the subsequent sections.

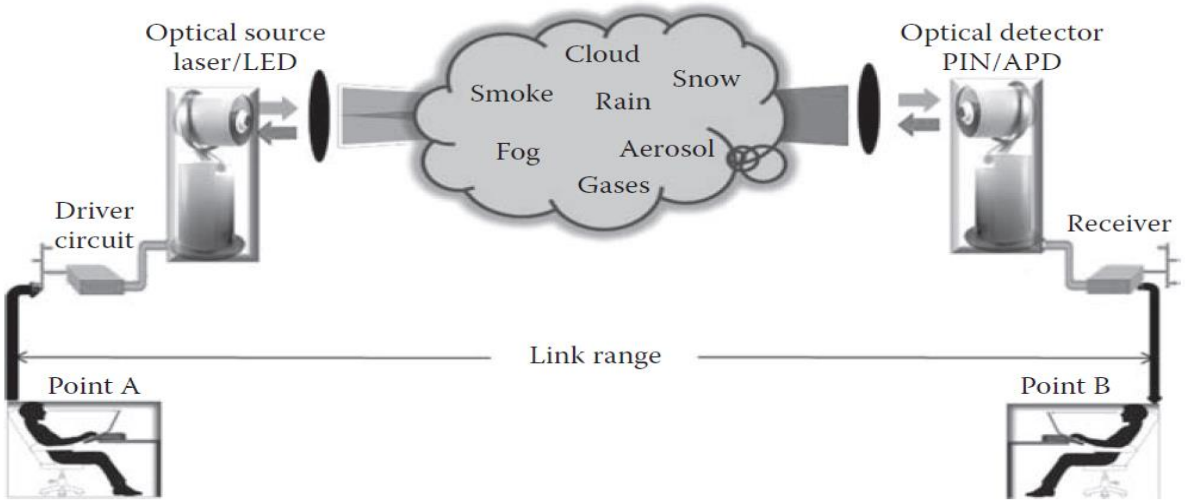

Figure 2-2: System model of FSO Outdoor Link

2.5.1 Transmitter

The transmitter helps to modulate the source data streams onto a carrier in terms of its frequency, intensity, phase etc. which are then transmitted over the atmospheric channel to the receiver. The intensity modulation (IM) scheme is conventionally used to modulate source data onto irradiance of the optical carrier. This can be realized by changing the optical source driving current in relation to the optical signal to be propagated or through the use of an external modulator, like Mach-Zender modulator. The adoption of external modulation ensures more data streams compared to the direct modulation. External modulation can also be employed to modulate various parameters of irradiance optical environment like frequency, phase, polarization status etc. with data/optical signals. The telescope of the transmitter accumulates, assembles and directs the optical irradiance to the telescope of the receiver at the opposite terminal of the channel. Table 2-1 below presents the summary of the generally adopted light sources in WOCS.

Table 2-1: Optical Light Sources

Wavelength	**Class**	**Inference**
850 nm	Vertical cavity surface emitting laser	Economical and accessible Absence of active cooling Lesser power density Accurate and available up to approximately 10 Gps Ideal power: 6 mW
1300 nm/1550 nm	Fabry-Perot laser	Durable Minimum eye safety requirement Immense power density i.e. 50times than 100 Mw/cm^2 Ideal power: 28 mW
	Distributed-feedback laser	Suitable for Erbium doped fibre amplifier Great speed about 40 Gps Gradient capability of 0.03-0.2 W/A Ideal power: up to 1-2 W when used with Erbium doped fibre amplifier [31].
10 000 nm	Quantum cascade laser	Costly and recently introduced Rapid and very responsive Components are scarce Inability to penetrate glass Better thin fog propagation properties [32]. Ideal output power: about 100 mW
Near Infrared	Light Emitting Diode (LED)	Not expensive Lesser and safe power density Non coherent Lesser data streams: <200 Mbps [33]. Ideal low power: <10 mW

Between the 700 nm and 10,000 nm wavelength range, there are numerous propagation windows that nearly fade out at attenuation of <0.2 dB/km. Most of the WOCS are being built to function at 780 nm-850 nm and 1520 nm-1600 nm spectral regions. The 1520 nm-1600 nm range is the most commonly adopted spectrum, since its equipment and units are easily accessible and very economical [29]. The 1550 nm wavelength is usually adopted for numerous purposes such as: (i) suitable for 3rd region wavelength-division

multiplexing (WDM) systems; (ii) Good eye safety criteria (allows higher power to be propagated compared to the 780 nm range); and (iii) minimizes solar background and irregularities during light haze or fog. Therefore, at 1550 nm more power can be conveyed to overcome the influence of attenuation due to fog [34]. However, the deficiency of the 1550 nm wavelength are lower detector sensitivity, expensive components and tough alignment specifications.

2.5.2 Atmospheric Channel

The atmospheric channel is made up of gases, shown in Table 2-2 below as well as aerosols, small molecules hanging in the air. Occasionally, there is also presence of precipitation such as fog, rain, haze etc. The volume of precipitation available in the air is location (longitude and latitude) and season dependent. The maximum concentration of molecules is found close to the earth core in the troposphere and it reduces with rising altitude up to the ionosphere [35].

Table 2-2: Atmospheric Gas constituents

Atmospheric Constituents	**Volume Ratio (%)**	**Piece Per Million (ppm)**
Nitrogen (N_2)	78.09	
Oxygen (O_2)	20.95	
Argon (Ar)	0.93	
Carbon dioxide (CO_2)	0.03	
Water vapour (H_2O)		40-40,000
Neon (Ne)		20
Helium (He)		5.2
Methane (CH_4)		1.5
Krypton (Kr)		1.1
Hydrogen (H_2)		1.0
Nitrogen oxide (N_2O)		0.6
Carbon monoxide (CO)		0.2
Ozone (O_3)		0.05
Xenon (Xe)		0.09

Optical signals travelling through the atmosphere are dispersed/lost resulting in loss of power due to the size of the atmospheric components. Some of the protons are being absorbed by the atmospheric constituents (fog, ozone, water vapor, carbon dioxide etc.) and their energy is transformed into heat energy. Although others may not experience loss of energy, however, their original line of transmission may be altered i.e. scattering [36]. The light beam also diffuses out while travelling through the atmospheric

medium hence increasing the volume of the received beam beyond the aperture diameter of the receiver [35].

2.5.3 Atmospheric Turbulence

When the sun's radiation reaches the earth's core, it warms up the (earth's) surface air volume. The resulting warm volume of air later expands and combines turbulently with the neighboring cooler air volume, thereby resulting in spatial and temporal changes in the atmospheric temperature over the line of transmission. The temperature variations depends on the altitude and wind speed. The temperature non-uniformity of the atmosphere results in a corresponding variation of the refractive index as well as fluctuations in the volume of cells ranging from ~0.1 cm - ~10 m. The traversing optical wave is therefore wholly or slightly deflected based on the volume of the light beam and the intensity of the temperature non-uniformity over the line of propagation. Thus, the optical radiation propagating through the turbulent air encounters irregular fluctuation/fading alongside its irradiance (i.e. scintillation) and the laser phase [37]. The Atmospheric turbulence depends on fluctuations of the refractive index, wind speed, altitude/pressure of the atmosphere.

The impacts of atmospheric turbulence on FSO communication systems includes [38]:

(a) Beam steering - Angular diversion of the optical beam from its original LOS path thereby making the beam to go out of the receiver radius.
(b) Image dancing - The received light beam focus shifts in the image plane as a result of the fluctuations of the laser angle of arrival.
(c) Beam spreading - The beam deviation is raised due to scattering, thus causes a decrease in the power density of the received signal.
(d) Beam scintillation – Fluctuations of the power density at the receiver area produced by small ratio of destructive interference in the cross section of the optical beam.
(e) Spatial coherence degradation – These are losses experienced in the phase coherence over the beam fronts due to turbulence [39].
(f) Polarization fluctuation - This occurs due to variations in the nature of the received optical field polarization having passed through a turbulent channel. It is inconsequential for the horizontally propagating optical radiation [40].

The statistical modelling of the received optical radiation propagating through a turbulent channel will be investigated in chapter three.

2.5.4 Receiver

The receiver is typically used to regain propagated data streams from the corresponding optical fields. It is made up of the following:

(a) Receiver Telescope: It receives and concentrates the approaching optical radiation towards the photo-detector. It is deduced that a wider receiver telescope diameter is needed to obtain numerous uncorrelated radiations and aligns them towards the photo-detector. This is known as aperture averaging though a large aperture diameter may cause further background noise.

(b) Optical band-pass filter: It helps to minimize the volume of background noise.

(c) Photo-detector: This is the Pin-diode (PIN)/avalanche photo-diode (APD) that transforms the approaching optical field into electrical signals. The generally employed photo-detectors in WOCS are highlighted in the Table 2-3.

(d) Post detection Processor: This helps to carry out the amplification, signal processing and filtering to obtain highly reliable data rates.

Table 2-3: WOCS Photo-detectors

Materials	**Wavelength (nm)**	**Responsivity**	**Ideal Sensitivity**	**Gain**
Silicon PIN	300-1100	0.5	-34 dBm at 155 Mbps	1
Silicon PIN (trans impedance amplifier)	300-1100	0.5	-26 dBm at 1.25 Mbps	1
InGaAs PIN	1000-1700	0.9	-46 dBm at 155 Mbps	1
Silicon APD	400-1700	77	-52 dBm at 155 Mbps	150
InGaAs APD	1000-1700	9	-33 dBm at 1.25 Gbps	10
Quantum-well/quantum-dot detectors	~10,000			

The detection process of the receiver can be categorized into:

Direct detection receiver: This is a kind of receiver that detects the instantaneous strength of the optical irradiance induced on the photo-detector. However the gain of the photo-detector corresponds to the power of the incident optical field. It is easy to deploy and more appropriate for intensity modulated optical networks [35, 38].

Coherent detection receiver: This is a type of receiver that works based on the photo-mixing mechanism. The approaching optical field is combined with other optical field that are obtained on the outer layer of the photo-detector. It can also be sub-divided into heterodyne and homodyne receivers. In heterodyne receiver, the wavelengths/frequencies of the host oscillator is different from that of the approaching radiations [35], whereas in homodyne detection, the approaching radiations and host oscillator wavelength/frequencies are

absolutely the same [41]. In comparison to radio frequency (RF) coherent receivers, the output of the host oscillator in optical coherent receiver is not required to have equal phase to the approaching radiations. The major qualities of a coherent detector are: SNR can be substantially increased by just raising the host oscillator power and the simple way of amplification at instantaneous frequency.

2.6 Eye Safety Standards

During the modelling of free space optical communication systems, adequate measures should be put in place to guarantee that the optical radiation will be safe and not harmful to users/anyone that might interact with the system. The optical radiations may cause damage to the eye and skin, though the injury to the eye is much more consequential due to the eye's ability to converge and focus optical energy. As stated by the revised IEC 60825-1 standard, the classification of laser in accordance with their important features and requirements is summarized in Table 2-4 [34].

Table 2-4: Classification of laser beams according to eye safety and standard

Laser Class	**Remarks**
Class 1	Lower power equipment which emits radiation at (302.5-4000 nm) wavelength. They are intrinsically not harmful based on their technical structure under proper usage situation such as using optical device (microscope, binocular, monocular etc.) to viewing.
Class 1M	It has similar features as class 1 but could be harmful when used with optical devices like telescope, binocular etc. and it also gives wide-diameter beams.
Class 2	It is lesser power device that emits radiation within (400-700 nm). Defense reflexes (palpebral reflex) are employed to protect the eye and can be used with optical equipment for viewing.
Class 2M	It also has lesser power device that emits radiation within (400-700 nm). Defense reflexes (palpebral reflex) are employed to protect the eye but can't be used with optical equipment for viewing.
Class 3R	Mean power equipment which emits radiations within (302.5-4000 nm) but direct exposure is harmful.
Class 3B	Mean power equipment which emits radiations within (302.5-4000 nm) but direct exposure is harmful. Medical measures and training are mandatory before deployment and maintenance of the system.
Class 4	Immense power technology. It is dangerous to the eye, skin and has high fire risk. Should be lock always with safety key switch. Medical measures and training are mandatory before deployment and maintenance of the system.

There are various international standard agencies that give support/guidelines on the safety matters of optical light beams, distinguished among these organizations are [31]: Center for Devices and Radiological Health (CDRH), International Electrotechnical Commission (IEC), American National Standards Institute (ANSI), European Committee for Electrotechnical Standardization (CENELEC), Laser Institute of America (LIA).

2.7 Summary

This chapter has reviewed the fundamentals of WOCS. The main characteristics and uses which enable WOCS to be suitable for the high capacity access networks were introduced. The various challenges encountered by the optical beam traversing through the atmospheric medium were also examined with the objective of having an ideal review of the WOCS and comparing it to RF as a link for wireless communication. Different scenarios of FSO applications were highlighted alongside the eye safety issues and optical laser classifications.

Chapter 3 – Methodological Approach

3.1 Introduction

This chapter examines and discusses the different statistical models used in this dissertation. These include a model for estimating the diverse losses encountered by optical signals during propagation in the atmosphere namely scattering, scintillation etc. The Log Normal model is employed to examine the influence of scintillation. Geometric loss due to beam divergence will be examined. Link margin and link availability will also be analyzed.

3.2 FSO Propagation Link Loss

The atmospheric medium weakens optical fields travelling through it by absorption and scattering phenomena. The higher constituents of particles in the air, which causes signal fading, fluctuates randomly and it depends on the present weather conditions. For a physical layer FSO communication link propagating optical signals through the atmosphere with a propagation link length *L* can be described by Beer-Lambert's law, which is given as [24]:

$$\tau(\lambda, L) = \frac{P_{rx}}{P_{tx}} = exp[-\gamma_{tx}(\lambda)L] \tag{3.1}$$

where $\tau(\lambda, L)$: Transmittance of the atmospheric medium at wavelength (λ)

P_{rx}: Received Power

P_{tx}: Transmitted Power

$\gamma_{tx}(\lambda)$: Attenuation/fading coefficient (m^{-1})

The fading of the optical signal in the atmospheric channel depends on the presence of molecular elements i.e. aerosols and gases. The fading coefficient is the summation of scattering and absorption coefficients from molecular elements in the air and aerosols, which is given as [29]:

$$\gamma_{tx}(\lambda) = \alpha_m(\lambda) + \alpha_a(\lambda) + \beta_m(\lambda) + \beta_a(\lambda) \tag{3.2}$$

$\alpha_a(\lambda)$ and $\alpha_m(\lambda)$: aerosol and molecular absorption coefficients
$\beta_a(\lambda)$ and $\beta_m(\lambda)$: aerosol and molecular scattering coefficients

Absorption occurs during interaction between transmitting photons and particles in the atmosphere on their line of propagation. Absorption coefficient depends on certain kinds of gases and their constituents. It is wavelength dependent and selective, thereby resulting in a band of wavelengths with little absorptions known as transmission/propagation windows as depicted in Table 3-1:

Table 3-1: Electromagnetic Spectrum

EM Spectrum	**Wavelength Range (mm)**
Visible and very-near Infrared	0.4 to 1.4
Near Infrared	1.4 to 1.9 and 1.9 to 2.7
Mean Infrared	2.7 to 4.3 and 4.5 to 5.2
Far Infrared	8 to 14
Extremely Infrared	16 to 28

Since it is impossible to alter the physics of the atmospheric channel, wavelengths are selected in FSO to correspond with the range of wavelengths with little absorption [31]. The fading coefficient is however dominated by scattering, thus

$$\gamma_{tx}(\lambda) \cong \beta_a(\lambda) \tag{3.3}$$

and $\alpha_m(\lambda)$ can therefore be ignored.

3.3 Fading due to Scattering

Scattering causes angular redistribution of optical signals and its impacts depends on the radius r of the molecules (i.e. aerosol, fog) encountered during transmission. For the size parameter:

$$m_0 = \left(\frac{2\pi r}{\lambda}\right) \tag{3.4}$$

When $m_0 \ll 1$, it is categorized as Rayleigh scattering; if $m_0 \approx 1$, it is referred to as Mie scattering while for $m_0 \gg 1$, it can be explained better using geometric optics. Mie scattering occurs when the molecule size is equivalent to the optical beam size and as the fog particle size compares to the wavelength range of concern in FSO technology ($0.5\ \mu m - 2\ \mu m$), this makes fog the main photo scattering molecule and Mie scattering becomes the dominant scattering process in physical layer WOCS. The optical field power loss as a result of Mie scattering is large in relation to snow and rain induced losses. The empirical Mie scattering theory is given as:

$$\gamma_{tx}(\lambda) \cong \beta_a(\lambda) = 10^5 \int_0^{\infty} Q_e\left(\frac{2\pi r}{\lambda}, \dot{n}\right) \pi r^2 n(r) dr \quad [dB/km] \tag{3.5}$$

where r represents the particle radius (aerosol, fog etc.) in centimeters, Q_e represents the Mie scattering efficiency, $\dot{n}$ represents the real part of the complex index of refraction while $n(r)$ represents the amount of fog molecules per unit volume for a unit rise in the radius. In this scenario, $\beta_a(\lambda)$ represents the specific attenuation estimated in dB/km and is determined by adding up the attenuation influence of all the respective fog particles available in the atmosphere per unit volume for a unit rise in radius.

Fading in the atmosphere is the reciprocal of the transmittance, which is defined by the Beer-Lambert law in equation 2.1 [42]. The atmospheric fading coefficient $\gamma_{tx}(\lambda)$ can be described as a function of meteorological visibility $V(km)$ i.e. $\gamma_{tx}(V)$, given as a function of link length where the transmittance has an absolute value ϵ i.e. $[\tau(L, V) = \epsilon]$. In 1924, Koschmeider proposes an optical threshold $\epsilon = 0.02$. The atmospheric fading coefficient can then be expressed as [43]:

$$\gamma_{tx}(V) = \frac{-\ln(0.02)}{V(km)} = \frac{3.91}{V(km)}, \tag{3.6}$$

The visibility range refers to the distance at which a lateral luminous optical beam propagates over in the atmospheric medium till its intensity falls to 2% of its initial value [44]. The values of atmospheric attenuation coefficient for fog and haze can be determined by:

$$\beta_a(\lambda) = \frac{10 \log_{10} I_{Th}}{V(km)} \left(\frac{\lambda}{\lambda_0}\right)^{-q} \tag{3.7}$$

$$\beta_a(\lambda) = \frac{-\ln(0.02)}{V(km)} \left(\frac{\lambda}{\lambda_0}\right)^{-q} = \frac{3.91}{V(km)} \left(\frac{\lambda}{\lambda_0}\right)^{-q} = \frac{3.91}{V(km)} \left(\frac{\lambda}{550nm}\right)^{-q}, \tag{3.8}$$

where $V(km)$ represents the visibility range, λ is the wavelength (nm), λ_0 denote the visibility range reference wavelength ($550\ nm$) and q represents the molecule size distribution coefficient of scattering in the atmosphere. Therefore, atmospheric fading in decibel per link length can be expressed as:

$$A_{att} = 4.343 \times \beta_a(\lambda) \quad [dB/km] \tag{3.9}$$

Therefore, we obtain Eqn. (3.10) by substituting Eqn. (3.8) into Eqn. (3.9):

$$A_{att} = \frac{16.98}{V(km)} \left(\frac{\lambda \times 10^{-9}}{550nm}\right)^{-q} \quad [dB/km] \tag{3.10}$$

The atmospheric fading due to scattering may be obtained from Eqn. (3.9) and (3.10), considering the fact that $\beta_a(\lambda)$ depends on wavelength and visibility. For wavelengths within the range of visible to near infrared light as well as visibility(km), it can be estimated using the semi empirical Kim and Kruse model modified for $\epsilon = 0.02$ such that:

Kim Model

$$q = \begin{Bmatrix} 1.6 \quad for\ v > 50km \\ 1.3 \quad for\ 6km < v < 50km \\ 0.16v + 0.34 \quad for\ 1km < v < 6km \\ v - 0.5 \quad for\ 0.5km < v < 1km \\ 0 \quad for\ v < 0.5km \end{Bmatrix} \tag{3.11}$$

Kruse Model

$$q = \begin{Bmatrix} 1.6 \quad for\ v > 50km \\ 1.3 \quad for\ 6km < v < 50km \\ 0.585V^{1/3} for\ 0 < v < 6km \end{Bmatrix} \tag{3.12}$$

The atmospheric visibility band and attenuation can be categorized for various weather conditions as shown in the Table 3-2 below [34]:

Table 3-2: International Visibility and Attenuation Code

Weather Conditions	**Visibility Range**	**Attenuation**
Thick Fog	0.2 km	75 dB/km
Moderate fog	0.5 km	28.9 dB/km
Light fog	0.770-1 km	18.3 dB/km
Thin fog/heavy rainfall ($25\ mm/hr$)	1.9-2 km	6.9 dB/km
Haze/medium rain ($12.5\ mm/hr$)	2.8-4 km	4.6 dB/km
Clear weather /drizzle ($12.5\ mm/hr$)	18-20 km	0.54 dB/km
Very clear weather	23-50 km	0.19 dB/km

The rate of the q parameter shows that atmospheric fading coefficient $\beta_a(\lambda)$ strongly depends on the optical field wavelength used for the entire atmospheric visibility range. The fading coefficient reduces as the wavelength increases.

Ferdinandov Model

Literature review shows that Ferdinandov was introduced by koschmeider generalization law for fog and has been adopted with average value of data. There is a satisfactory difference between the Ferdinandov, Kim and Naboulsi model for wavelength range of $(0.3 - 1.1\ \mu m)$. It can be expressed as [45]:

$$F_{\propto}(\lambda) = a(\lambda)V^{-q(\lambda)}[km^{-1}] \tag{3.13}$$

$$q(\lambda) = 0.199\ln(\lambda) + 1.157$$

$$a(\lambda) = -2.656\ln(\lambda) + 2.449$$

3.4 FSO Measurements of Durban

The easy and successful deployment of FSO systems in eastern coast of South Africa depends mostly on the local weather conditions. Hourly visibility data for eastern coast of South Africa was captured at the King Shaka International Airport daily over the period of six years (i.e. 2010, 2011, 2012, 2013, 2014 and 2015). Figure 3-1, shows major locations under research with similar average weather conditions to other areas in the eastern coast of South Africa (i.e. Richards Bay, East London etc.).

Figure 3-1: Map of Durban showing major locations under research.

3.5 Atmospheric Turbulence Losses

The optical fields propagating through the atmospheric medium may be attenuated under clear skies conditions without the influence of scattering and absorption, due to a quantity known as refractive index of atmospheric turbulence. It depends on the altitude of the FSO transceiver above the ground level and can be evaluated by using the modified Hufnagel-Valley (H-V) model expressed as [46]:

$$C_R{}^2 = 0.00594\left(\frac{wp}{27}\right)^2 (10^{-5}a)exp\left(\frac{-a}{1000}\right) + (2.7\times 10^{-16})exp\left(\frac{-a}{1500}\right) + T_I\left(\frac{-a}{100}\right) \qquad (3.14)$$

Where $C_R{}^2$ is the refractive index in $(m^{-2/3})$ which depends on location, time, relative humidity, temperature, pressure, wind speed and so on, wp represents wind speed in (ms^{-1}), a denotes altitude in meters (m) and T_I represents the turbulence intensity on the ground (1.7×10^{-14}).

3.5.1 Scintillation

This is the temporal and spatial fluctuations of irradiance caused by atmospheric turbulence in FSO link which heavily distorts optical beams [47]. The strength of scintillation impacts is captured by the Rytov model and is called scintillation index [48]. Scintillation index is used to estimate the volume of turbulence loss over the FSO link length. In this dissertation, weak turbulence is considered over the line of propagation. For plane waves under weak turbulence, the scintillation index is given as [49]:

$$S_I = 1.23{C_R}^2 k^{7/6} L^{11/6} \tag{3.15}$$

Where $k = \frac{2\pi}{\lambda}$ represents the optical wave number in (m^{-2}). The average aperture is primarily produced by minor fluctuations in temperature and pressure in the air, which causes random fluctuations in the refractive index. Therefore, scintillation attenuation can also be estimated as [19]:

$$S_{att} = \left|10\log\left(1 - \sqrt{S_I}\right)\right| \quad [dB] \tag{3.16}$$

3.5.2 Log-Normal Model

This is a statistical distribution adopted to model weak atmospheric turbulence. In this dissertation, the Log normal model was used to obtain an expression to determine the required margin to compensate for power losses in optical signals due to scintillation. The probability density function (pdf) of the received optical signal power is given as [50]:

$$P(X) = \frac{1}{2} erfc\left[\frac{-\ln x - \mu_x}{{s_d}^2\sqrt{2}}\right] \tag{3.17}$$

Where $erfc$ represents the error complementary function, ${s_d}^2$and μ_x represents the standard deviation and mean respectively of the lognormal (pdf). The power scintillation index for the received signal can be expressed as [51]:

$$P_{scin} = exp({s_d}^2) - 1 \tag{3.18}$$

When normalized at $x = P_{rx}$;

$$P_{scin} = exp({s_{rx}}^2 + 1) \tag{3.19}$$

The required margin for power loss compensation in optical systems due to scintillation depends on the power scintillation index and outage probability of the FSO system. It is expressed as:

$$F_m = 10\log\left[exp\left(\sqrt{2\ln({s_{rx}}^2+1)}\right)erfc^{-1}(2P_{scin}) - 0.5\ln({s_{rx}}^2+1)\right] \quad [dB] \tag{3.20}$$

Where P_{scin} and F_m are the power scintillation index and the required compensation margin for losses due to scintillation in the atmosphere.

3.5.3 Optical beam Divergence Loss

One of the major merits of FSO over RF systems is its ability to transmit a very tiny optical beam, hence offers a highly secure network. Diffraction is a process whereby an optical beam spreads out, which results in a wider spread of the signal making it difficult for the receiver aperture to capture all the transmitted beam.

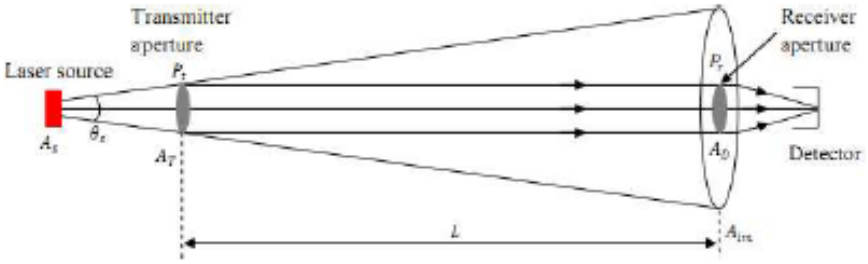

Figure 3-2: Beam Divergence

Considering an optical laser source that is small and non-diffuse, as depicted in Figure 3.2, the ratio of the received power to the transmitted power can be calculated as:

$$\frac{P_r}{P_t} = \frac{A_D}{A_{im}} = \frac{{d_R}^2}{(d_T + \theta_s L)^2}, \tag{3.21}$$

where d_R and d_T are the receiver and transmitter diameters, respectively. A_{im} represents the diffraction pattern size, L denotes the link length, θ_s represents the divergence angle of the optical laser source. A_D, A_T, and A_s denotes the aperture area of the receiver, transmitter and source respectively. The geometric loss G_{loss} can be expressed as:

$$G_{loss} = -20\log\left[\frac{d_R}{(d_T + \theta_s L)}\right] \quad [dB] \tag{3.22}$$

It is observed from equation 3.21 that the geometric loss reduces as the receiver aperture area expands and the divergence angle decreases. However, the geometric loss also increases with the rise in the transmission

link length. Therefore, a very narrow angle of divergence is recommended for a source with a large angle of divergence in physical layer FSO systems.

3.6 FSO Link Margin and Availability

The beam divergence angle, mean optical laser power, receiver sensitivity, coupling losses, and aperture diameter are parameters that determine how FSO system is able to minimize atmospheric influences. These FSO system parameters determine the link margin and are outlined in the table 3-3 [52].

Table 3-3: FSO system Parameters

System Parameters	**Typical Value**
Optical Laser Power (P_m)	16 dBm
Receiver Sensitivity (P_{rs})	-38 dBm
Coupling losses $(A_T + A_R)$	6 dB
Beam Divergence Angle (θ)	2.8 mrad
Aperture Diameter (D_A)	160 mm
Transmit Optical Output	40 mW/16 dBm
Wavelength	850 nm
Receiver Detector	Avalanche Photo Diode (APD) 50 or 0.4 A/W
Receiver field of view (FOV)	10 mrad
Eye Safety	Class 1M

Taking into consideration the value of the system parameters mentioned in table 3.3 above, the link margin may be estimated through equation (3.23) given as [19]:

$$(M_L) = P_m - A_T - 20\log\left(\frac{\sqrt{2}L\theta}{D_A}\right) - A_R - P_{rs} \quad [dB], \tag{3.23}$$

From equation 3.23;

$$20\log\left(\frac{\sqrt{2}L\theta}{D_A}\right) = 20\left[\log\sqrt{2} + \log L + \log\theta - \log D_A\right],$$

$$20\log\left(\frac{\sqrt{2}L\theta}{D_A}\right) = 20\left[\log\sqrt{2} + \log\theta - \log D_A\right] + 20\log L,$$

$$20\log\left(\frac{\sqrt{2}L\theta}{D_A}\right) = 20\log\left(\frac{\sqrt{2}\theta}{D_A}\right) + 20\log L, \tag{3.24}$$

Therefore;

$$(M_L) = P_m - A_T - 20\log\left(\frac{\sqrt{2}\theta}{D_A}\right) - 20\log L - A_R - P_{rs} \quad [dB], \tag{3.25}$$

$$(M_L) = 16 - 3 - 20\log\left(\frac{\sqrt{2} \times 2.8 \times 10^{-3}}{0.16}\right) - 20\log L - 3 - (-38)$$

$$(M_L) = 13 - 20\log\left(\frac{\sqrt{2} \times 2.8 \times 10^{-3}}{0.16}\right) - 20\log L + 35$$

$$(M_L) = 48 - 20\log\left(\frac{\sqrt{2} \times 2.8 \times 10^{-3}}{0.16}\right) - 20\log L$$

$$(M_L) = 48 - 20\log(0.024748) - 20\log L$$

$$(M_L) = 48 + 32 - 20\log L$$

$$(M_L) = 80 - 20\log L \tag{3.26}$$

Thus;

$$(M_L) = M_0 - 20\log L\,[dB]. \tag{3.27}$$

Where $M_0 = 80$ and consists of all values of the system parameters in table 3.3 extracted from the FSO transceiver equipment and L is the link length (km). The optical link margin describes the amount by which an FSO system can compensate for losses due to scattering and turbulence for a given link length [31]. An FSO system with link length L will work reliably if:

$$(M_L)^* \geq A_{att}(L)^*. \tag{3.28}$$

Where $A_{att}(L)^*$ represents atmospheric losses i.e. summation of turbulence and scattering for link length$(L)^*$. Assuming the link length is in kilometers, the required minimum visibility V_{min} for reliable operation of the FSO system is expressed as [19]:

$$V_{mi} = \frac{13(L)^*}{(M_L)^*}\left(\frac{\lambda \times 10^{-9}}{550nm}\right)^{(-q(V))} \quad [km] \tag{3.29}$$

If the received power drops below the sensitivity of the receiver, the FSO optical link would be unavailable. The link availability strongly depends on the atmospheric conditions and it can be statistically expressed as [19]:

$$\begin{aligned} L_{avail} &= Probability[(M_L)^* \geq A_{att}(L)^*] \\ &= Probability[V \geq V_{mi}] \\ L_{avail} &= 1 - F_C[V_{mi}] \end{aligned} \tag{3.30}$$

3.7 Summary

In this chapter, FSO propagation losses were modelled using the Beer-Lambert theory to evaluate the absorption and scattering of optical signals in the atmosphere. The Kruse, Kim and Ferdinandov models were used to determine the atmospheric attenuation for Durban, South Africa. Effects of scintillation were also evaluated and an expression to determine the margin required to compensate for scintillation effects was obtained. The FSO system's optical beam divergence, link margin and link availability were discussed as well.

Chapter 4 – Results and Discussions

4.1 Introduction

In this chapter, we evaluate and present the visibility patterns from which the atmospheric attenuation coefficients of physical layer FSO systems can be determined for the eastern coast of South Africa. The effects of scattering and scintillation are also examined. The probability of encountering and exceeding atmospheric attenuation is investigated, and finally, the FSO link budget and link availability for the eastern coast of South Africa is estimated.

4.2 FSO Atmospheric Losses

Absolute FSO atmospheric losses are estimated by the summation of losses due to scattering and scintillation. From chapter 3, it is pointed out that scattering losses depends strongly on visibility. Furthermore, atmospheric turbulence losses are altitude and wind speed dependent. Considering these losses, this dissertation examines the performance of FSO communication systems for the eastern coast of South Africa. The visibility data captured daily for the period of January 2010 through December 2015 were used to determine the minimum, average and maximum annual attenuations of optical signals. Figure 4-1 shows the minimum, average and maximum visibility patterns for the eastern coast of South Africa over the period of six (6) years.

Figure 4-2 shows that the year 2014 recorded the lowest value of annual minimum visibility, which is found to be lower in May of 2010 while the year 2011 recorded the highest value of annual minimum visibility. It tends to be much higher from January to March for the eastern coast of South Africa over the period of six years. Figure 4-3 shows that the year 2014 recorded the lowest value of annual average visibility, with smaller values observed in May while during 2010-2012 the highest value of annual average visibility was recorded to be about 20 km for the eastern coast of South Africa over the period of six years. Figure 4-3 shows that the year 2011 recorded the highest value of annual maximum visibility of about 23 km, with the highest value in November while in 2014 the lowest value of annual maximum visibility of about 20 km was recorded for the eastern coast of South Africa over the period of six years. It is also observed that the month of May shows an anomaly in its visibility for the eastern coast of South Africa over the period of six years. The results are given in table 4-1, 4-2 and 4-3.

Table 4-1: Minimum Visibility Patterns for eastern coast of South Africa (2010-2015)

Minimum Visibility Patterns (2010-2015)							
Month	**2010**	**2011**	**2012**	**2013**	**2014**	**2015**	**Average**
January	19.526	19.357	18.681	16.822	19.019	16.146	18.2585
February	19.357	19.357	19.357	16.822	16.315	18.174	18.23033333
March	18.512	19.019	18.85	18.85	17.667	18.343	18.54016667
April	14.963	16.146	17.836	15.808	14.963	16.653	16.0615
May	14.963	16.146	15.977	11.076	7.02	14.456	13.273
June	14.287	15.639	14.456	13.949	14.118	11.414	13.97716667
July	14.625	16.484	14.625	15.132	12.597	15.132	14.76583333
August	13.949	17.329	13.78	14.118	13.442	13.273	14.31516667
September	13.949	16.484	16.991	14.456	16.484	15.808	15.69533333
October	16.991	17.667	19.526	15.977	16.822	17.16	17.35716667
November	18.005	18.512	18.85	16.822	17.16	14.963	17.38533333
December	18.512	19.019	19.188	18.512	18.005	17.498	18.45566667
Average	16	18	17	16	15	16	16.33333333

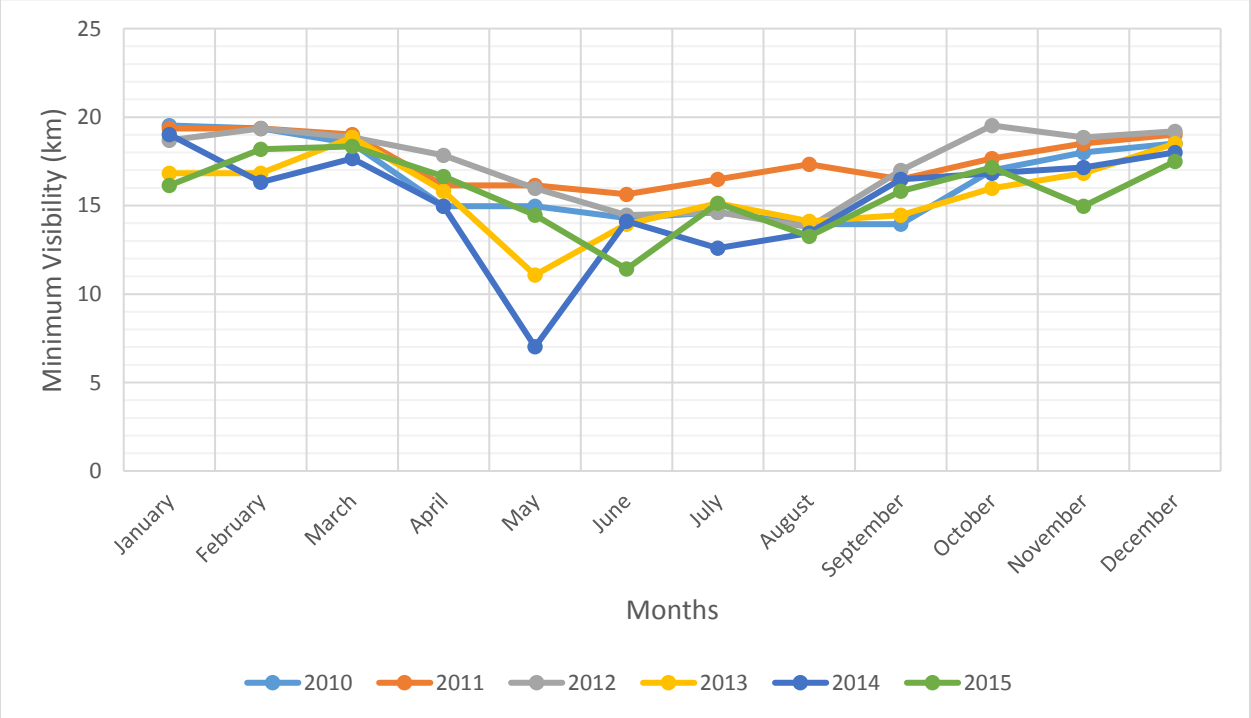

Figure 4-1: Annual Minimum Visibility patterns eastern coast of South Africa (2010-2015)

Table 4-2: Average Visibility Patterns for eastern coast of South Africa (2010-2015)

Average Visibility Patterns (2010-2015)							
Month	**2010**	**2011**	**2012**	**2013**	**2014**	**2015**	**Average**
January	20.709	21.216	20.709	19.864	20.371	19.695	20.42733333
February	20.371	20.202	20.878	19.526	18.85	19.864	19.9485
March	20.202	20.878	20.878	20.54	19.695	20.033	20.371
April	19.695	19.357	19.695	18.681	17.667	19.526	19.1035
May	19.526	19.357	18.681	16.653	7.02	18.681	16.653
June	18.343	19.019	18.343	17.667	17.498	16.653	17.9205
July	18.174	19.695	18.005	18.343	16.315	18.512	18.174
August	18.005	19.695	18.005	17.16	17.498	18.512	18.14583333
September	19.526	19.526	20.033	18.174	18.85	19.357	19.24433333
October	20.202	20.202	21.385	19.188	19.357	19.357	19.9485
November	20.709	21.047	20.709	19.695	19.357	18.85	20.06116667
December	21.216	20.878	20.878	20.54	19.864	19.864	20.54
Average	20	20	20	19	18	19	19.33333333

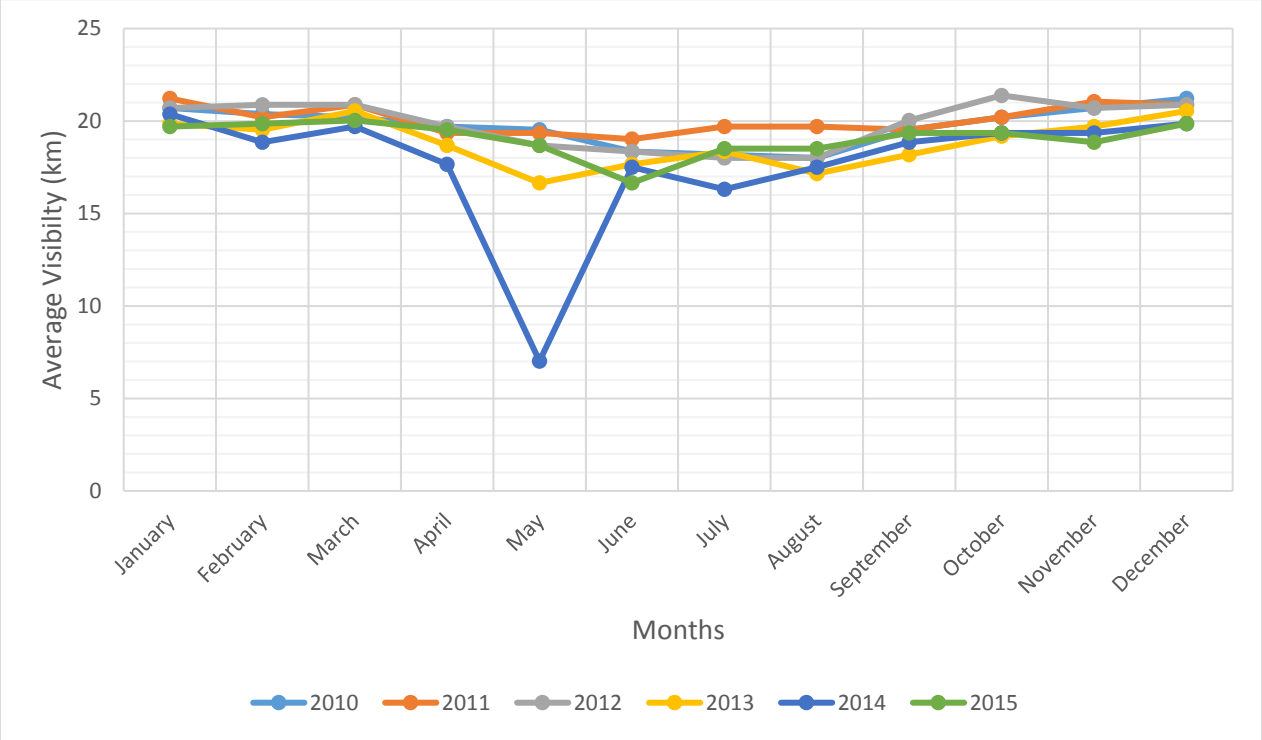

Figure 4-2: Annual Average Visibility patterns for eastern coast of South Africa (2010-2015)

Table 4-3: Maximum Visibility Patterns for eastern coast of South Africa (2010-2015)

Maximum Visibility Patterns (2010-2015)							
Month	**2010**	**2011**	**2012**	**2013**	**2014**	**2015**	**Average**
January	22.399	23.075	22.906	22.906	21.892	21.047	22.37083333
February	22.23	21.216	22.399	22.23	21.554	20.878	21.75116667
March	21.385	22.568	22.906	22.23	21.892	21.216	22.03283333
April	21.047	22.737	21.554	21.554	20.371	21.047	21.385
May	21.554	22.568	21.554	22.061	7.02	20.202	19.15983333
June	21.047	22.23	23.244	21.554	20.878	20.54	21.58216667
July	20.371	22.737	21.385	21.385	20.033	22.061	21.32866667
August	20.709	22.23	22.23	20.371	21.554	20.709	21.3005
September	21.216	22.399	23.244	21.892	21.216	21.892	21.9765
October	21.892	22.906	23.413	22.399	21.723	20.54	22.1455
November	22.23	23.582	22.568	22.399	21.723	21.892	22.399
December	23.244	22.568	22.399	22.568	21.723	22.23	22.45533333
Average	22	23	22	22	20	21	21.66666667

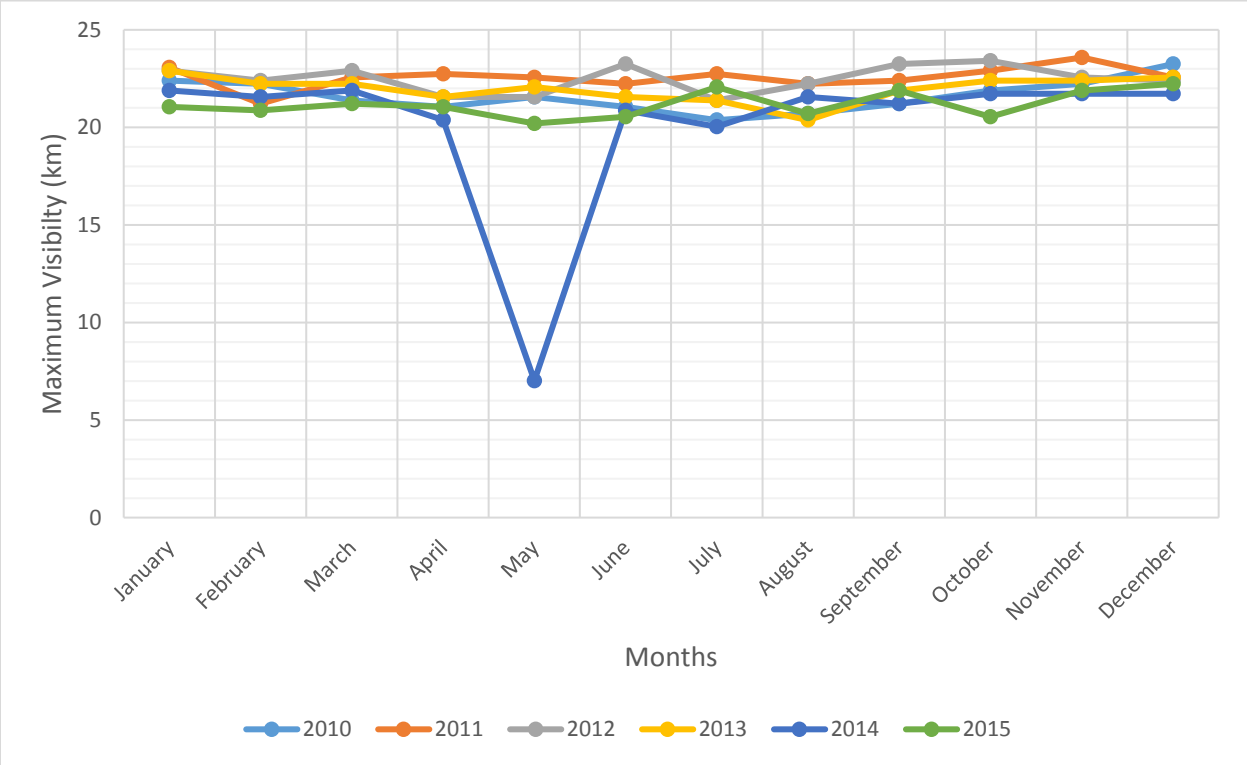

Figure 4-3: Annual Maximum Visibility patterns for eastern coast of South Africa (2010-2015)

4.2.1 Attenuation Coefficients Due to Scattering

Based on the recorded annual minimum, average and maximum visibility values for the eastern coast of South Africa (2010-2015) from figure 4-1, 4-2 and 4-3, the annual minimum, average and maximum scattering attenuation coefficients have been obtained using the Kim model at different wavelengths (that is 850 nm, 950 nm and 1550 nm) over the period of six years for the eastern coast of South Africa (see figure 4-4, 4-5 and 4-6). From Figure 4-1, 4-2 and 4-3, the years which recorded high values of visibility exhibit low scattering attenuation coefficients while those which recorded low values of visibility experience high scattering attenuations over the period of six years. It is also observed that the attenuation coefficients decreases as the wavelength increases from 850 nm to 1550 nm, which confirms that scattering attenuation coefficients depends strongly on the optical field propagation wavelength. The results are given in table 4-4, 4-5 and 4-6.

Table 4-4: Scattering Attenuation Coefficient 850 nm

Average Values (2010-2015)			
Scattering Attenuation Coefficient 850 nm			
Month	**Minimum**	**Average**	**Maximum**
January	0.43196	0.47288	0.38026
February	0.44412	0.48442	0.4818
March	0.43846	0.4741	0.36942
April	0.45191	0.50608	0.48243
May	0.60233	0.66356	0.33301
June	0.44807	0.53964	0.72485
July	0.45345	0.53281	0.4106
August	0.45375	0.53302	0.50166
September	0.4397	0.5021	0.32208
October	0.43667	0.4846	0.53357
November	0.43127	0.48198	0.36372
December	0.43006	0.47028	0.47318
Average	0.45515	0.51212	0.44642

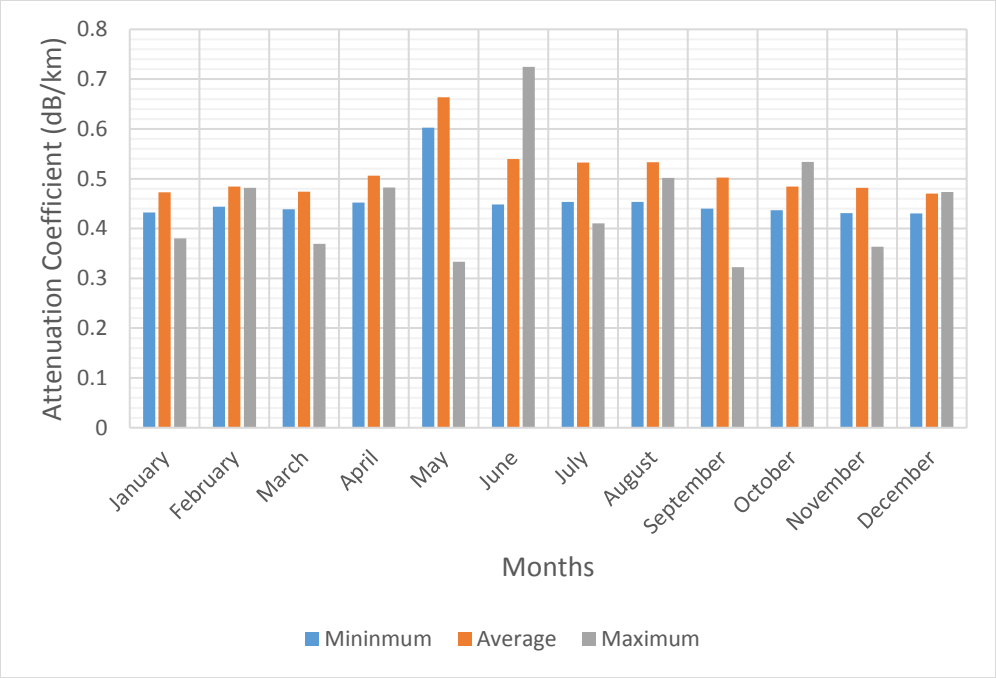

Figure 4-4: Attenuation Coefficient (dB/km) for eastern coast of South Africa (2010-2015) at 850 nm

Table 4-5: Scattering Attenuation Coefficient 950 nm

Average Values (2010-2015)			
Scattering Attenuation Coefficient 950 nm			
Month	**Minimum**	**Average**	**Maximum**
January	0.37381	0.40922	0.30993
February	0.38433	0.41921	0.36138
March	0.37944	0.41027	0.25082
April	0.39108	0.43795	0.37874
May	0.52124	0.57423	0.2066
June	0.38775	0.46699	0.60801
July	0.3924	0.46108	0.2682
August	0.39267	0.46126	0.38946
September	0.3805	0.43451	0.21408
October	0.37788	0.41936	0.42174
November	0.37322	0.4171	0.2513
December	0.37217	0.40697	0.48127
Average	0.39387	0.44318	0.34512

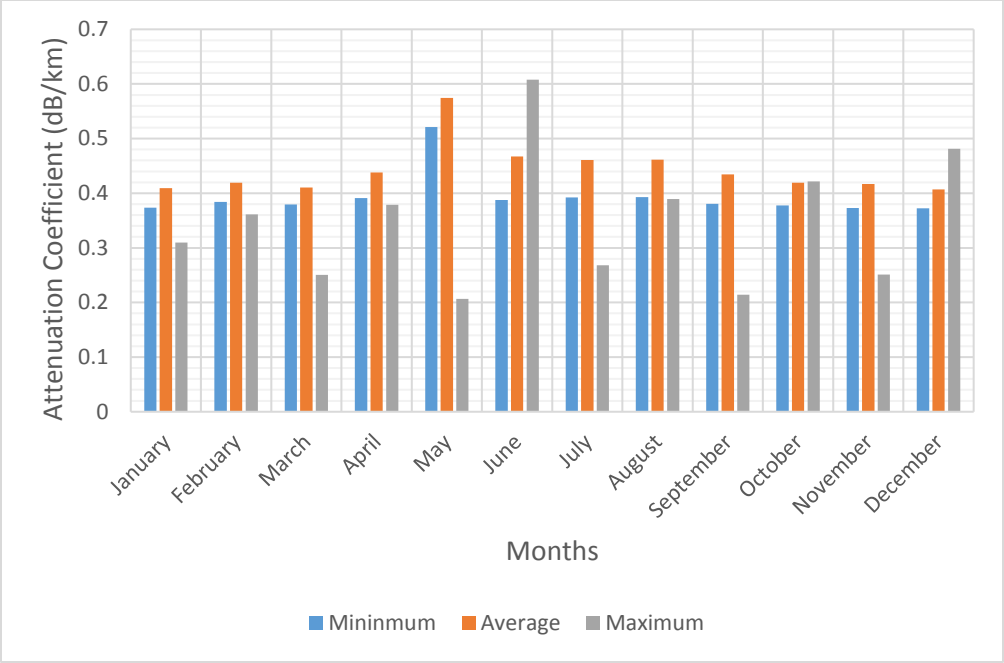

Figure 4-5: Attenuation Coefficient (dB/km) for eastern coast of South Africa (2010-2015) at 950 nm

Table 4-6: Scattering Attenuation Coefficient 1550 nm

Average Values (2010-2015)			
Scattering Attenuation Coefficient 1550 nm			
Month	**Minimum**	**Average**	**Maximum**
January	0.19782	0.21656	0.13809
February	0.20338	0.22184	0.17588
March	0.20079	0.21711	0.0994
April	0.20695	0.23176	0.25904
May	0.27584	0.30388	0.0576
June	0.20519	0.24713	0.45973
July	0.20766	0.244	0.073
August	0.2078	0.2441	0.25647
September	0.20136	0.22994	0.07925
October	0.19997	0.22192	0.27866
November	0.1975	0.22072	0.10621
December	0.19695	0.21536	0.31894
Average	0.20843	0.23453	0.19185

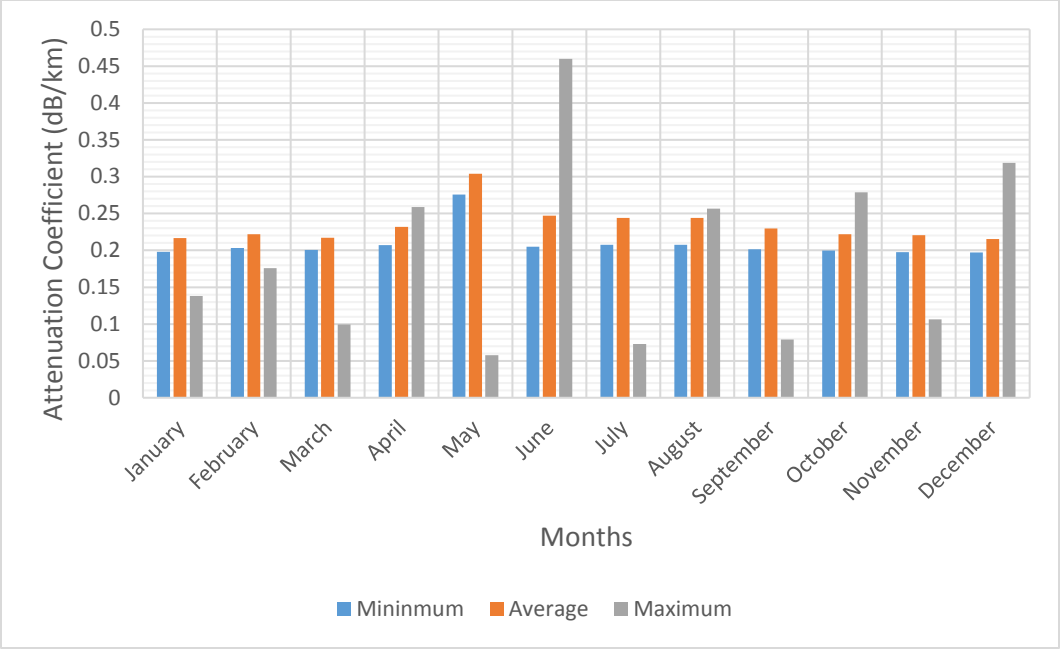

Figure 4-6: Attenuation Coefficient (dB/km) for eastern coast of South Africa (2010-2015) at 1550 nm

4.3 FSO Power Loss

The FSO power loss due to atmospheric scattering and scintillation has been estimated under clear sky. Table 4-7, 4-8 and 4-9 gives the scattering attenuation coefficients for the eastern coast of South Africa at 850 nm, 950 nm and 1550 nm respectively.

Figure 4-7 and 4-8 compare and show the contribution of scattering, modelled with Ferdinandov and Kim distribution, and turbulence losses for 850 nm and 950 nm wavelengths to the overall atmospheric losses. It is observed that the eastern coast of South Africa experiences great scintillation losses due to its low mean atmospheric turbulence loss and altitude. However, a little reduction is noted in the peak of the scintillation with increase in the wavelengths from 850 nm to 950 nm and vice versa. It is also observed that Ferdinandov and Kim modelled scattering has minimal contribution to the total atmospheric loss while atmospheric turbulence (i.e. scintillation) due to its peak values, is the major contributor to the attenuation of propagating optical signals and poor performance of the FSO link in the eastern coast of South Africa.

In Figure 4-7, the Kim model was adopted to estimate the atmospheric attenuation at 850 nm wavelength, and it shows that the attenuation due to scattering contributes 9.47% to the absolute atmospheric losses while the atmospheric turbulence loss contributes 90.53% to the overall power loss for a link range of 4 km. Figure 4-7 also shows that using the Ferdinandov model for a link range of 4 km at 850 nm wavelength, the attenuation due to scattering contributes 8.60% to the total power loss while the atmospheric turbulence loss contributes 91.40% to the overall power loss. The results are given in table 4-7, 4-8 and 4-9.

Table 4-7: Atmospheric Attenuation for eastern coast of South Africa - (850 nm)

Atmospheric Attenuation- (850 nm)			
Distance (km)	**Ferdinandov et al Model - Atmospheric Scattering Losses (dB)**	**Kim Model - Atmospheric Scattering Losses (dB)**	**Atmospheric Turbulence Losses (dB)**
0.50	0.23065	0.25606	2.9115
1.00	0.4613	0.51212	5.49617
1.50	0.69195	0.76818	7.97035
2.00	0.9226	1.02424	10.37539
2.50	1.15325	1.2803	12.7303
3.00	1.3839	1.53636	15.04602
3.50	1.61455	1.79242	17.32964
4.00	1.8452	2.04848	19.58613
4.50	2.07585	2.30454	21.81918
5.00	2.3065	2.5606	24.03161
5.50	2.53715	2.81666	26.22565
6.00	2.7678	3.07272	28.4031
6.50	2.99845	3.32878	30.56546
7.00	3.2291	3.58484	32.714
7.50	3.45975	3.8409	34.84977
8.00	3.6904	4.09696	36.9737
8.50	3.92105	4.35302	39.08659
9.00	4.1517	4.60908	41.18914
9.50	4.38235	4.86514	43.28197
10.00	4.613	5.1212	45.36564
10.50	4.84365	5.37726	47.44064
11.00	5.0743	5.63332	49.50743
11.50	5.30495	5.88938	51.56639
12.00	5.5356	6.14544	53.61791
12.50	5.76625	6.4015	55.66231
13.00	5.9969	6.65756	57.69991
13.50	6.22755	6.91362	59.73098
14.00	6.4582	7.16968	61.7558
14.50	6.68885	7.42574	63.7746
15.00	6.9195	7.6818	65.7876

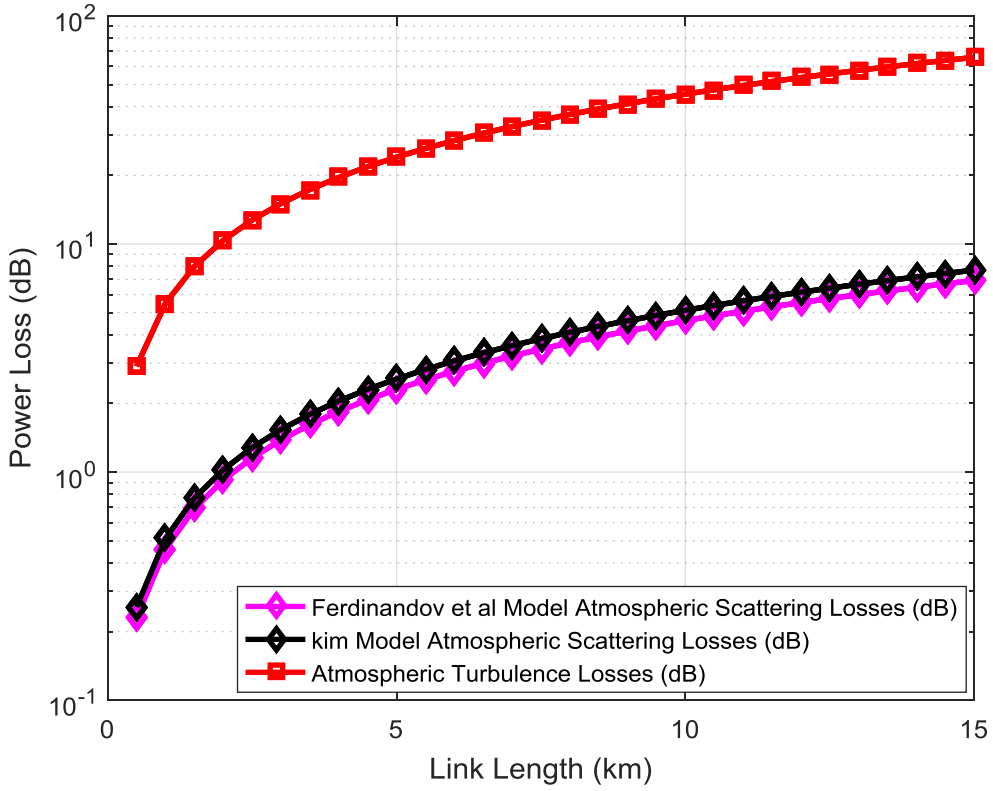

Figure 4-7: Atmospheric Attenuation due to scattering and turbulence for eastern coast of South Africa at 850 nm

Figure 4-8 shows that using the Ferdinandov model for a link range of 4 km at 950 nm wavelength, the attenuation due to scattering contributes 8.81% to the total power loss while the atmospheric turbulence loss contributes 91.19% to the overall power loss. Figure 4-8 also shows that using Ferdinandov model, the atmospheric attenuation at 950 nm wavelength due to scattering contributes 7.80% to the absolute atmospheric losses while the atmospheric turbulence loss contributes 92.20% to the overall power loss for a link range of 4 km.

Table 4-8: Atmospheric Attenuation for eastern coast of South Africa - (950 nm)

Attenuation for Durban- (950nm)			
Distance (km)	**Ferdinandov et al Model - Atmospheric Scattering Losses (dB)**	**Kim Model - Atmospheric Scattering Losses (dB)**	**Atmospheric Turbulence Losses (dB)**
0.50	0.19407	0.22159	2.72859
1.00	0.38813	0.44318	5.15089
1.50	0.5822	0.66477	7.46964
2.00	0.77626	0.88636	9.72359
2.50	0.97033	1.10795	11.93056
3.00	1.16439	1.32954	14.1008
3.50	1.35846	1.55113	16.24096
4.00	1.55252	1.77272	18.3557
4.50	1.74659	1.99431	20.44847
5.00	1.94065	2.2159	22.52191
5.50	2.13472	2.43749	24.57811
6.00	2.32878	2.65908	26.61877
6.50	2.52285	2.88067	28.64529
7.00	2.71691	3.10226	30.65885
7.50	2.91098	3.32385	32.66045
8.00	3.10504	3.54544	34.65095
8.50	3.29911	3.76703	36.6311
9.00	3.49317	3.98862	38.60157
9.50	3.68724	4.21021	40.56293
10.00	3.8813	4.4318	42.5157
10.50	4.07537	4.65339	44.46035
11.00	4.26943	4.87498	46.39729
11.50	4.4635	5.09657	48.32691
12.00	4.65756	5.31816	50.24954
12.50	4.85163	5.53975	52.16552
13.00	5.04569	5.76134	54.07511
13.50	5.23976	5.98293	55.97859
14.00	5.43382	6.20452	57.8762
14.50	5.62789	6.42611	59.76817
15.00	5.82195	6.6477	61.65472

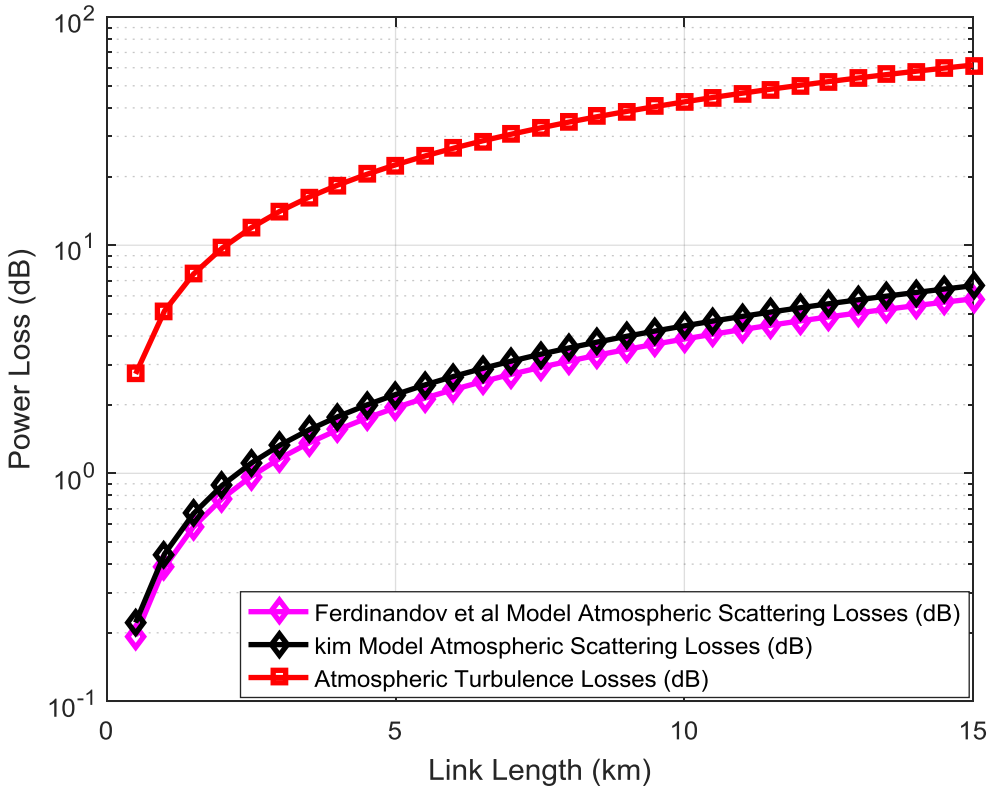

Figure 4-8: Atmospheric Attenuation due to scattering and turbulence for eastern coast of South Africa at 950 nm

Figure 4-9 shows that for a link range of 4 km at 1550 nm wavelength, the attenuation due to Mie scattering contributes 6.37% to the total power loss while the atmospheric turbulence loss contributes 93.63% to the overall power loss. The results obtained from figure 4-7, 4-8 and 4-9 has shown that atmospheric turbulence or scintillation are the major contributors to the attenuation of optical signals traversing the FSO atmospheric channel.

Table 4-9: Atmospheric Attenuation for eastern coast of South Africa using Kim model- (1550 nm)

Kim Model - (1550 nm)		
Distance (km)	**Atmospheric Scattering Losses (dB)**	**Atmospheric Turbulence Losses (dB)**
0.50	0.11727	2.05077
1.00	0.23453	3.87134
1.50	0.3518	5.61408
2.00	0.46906	7.30812
2.50	0.58633	8.96684
3.00	0.70359	10.59796
3.50	0.82086	12.20648
4.00	0.93812	13.79589
4.50	1.05539	15.36878
5.00	1.17265	16.92715
5.50	1.28992	18.47256
6.00	1.40718	20.00629
6.50	1.52445	21.5294
7.00	1.64171	23.04276
7.50	1.75898	24.54713
8.00	1.87624	26.04316
8.50	1.99351	27.53142
9.00	2.11077	29.01239
9.50	2.22804	30.48652
10.00	2.3453	31.9542
10.50	2.46257	33.41577
11.00	2.57983	34.87155
11.50	2.6971	36.32182
12.00	2.81436	37.76685
12.50	2.93163	39.20686
13.00	3.04889	40.64209
13.50	3.16616	42.07272
14.00	3.28342	43.49894
14.50	3.40069	44.92092
15.00	3.51795	46.33881

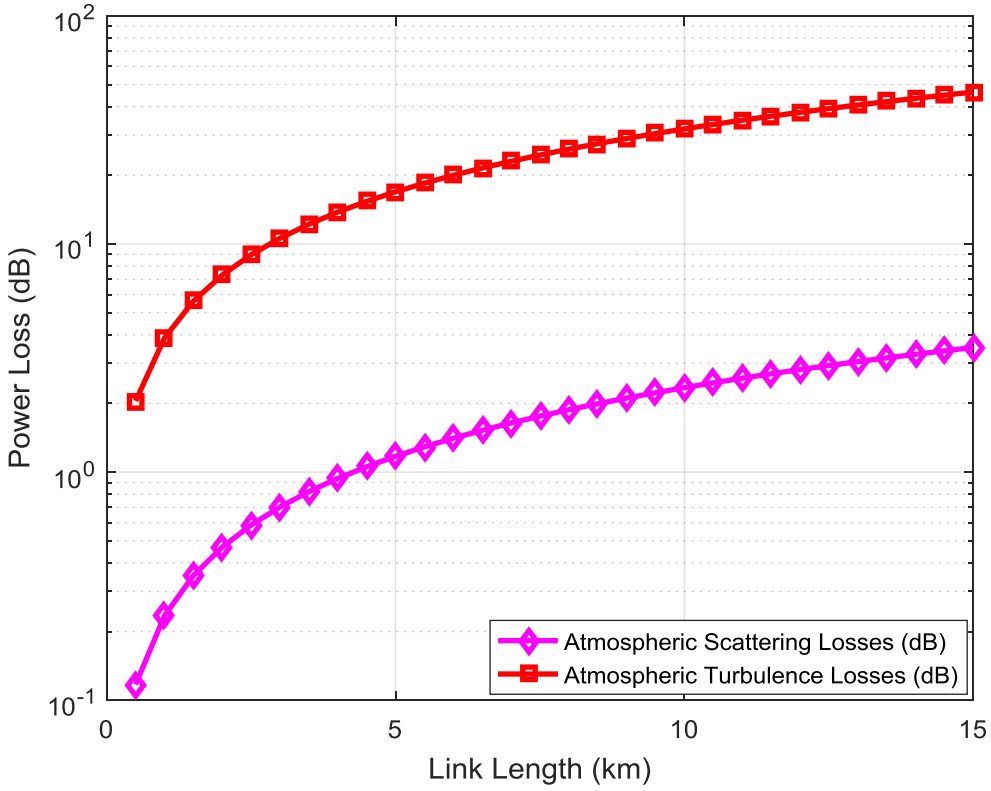

Figure 4-9: Atmospheric Attenuation due to scattering and turbulence using Kim model for eastern coast of South Africa at 1550 nm

Figure 4-10 shows the graph of the link margin and atmospheric scattering losses at different wavelengths against link length for the eastern coast of South Africa. Optimal link lengths along with their respective link margin values have been captured from the point where the power link margin intersects the corresponding average scattering atmospheric loss line. From figure 4-10, the Kim model at 1550 nm wavelength shows the longest FSO link length of 3 km at an atmospheric loss of 11.3 dB, followed by Ferdinandov et al and Kim Model (950 nm) at 2.5 km with 12.9 dB and 13.0 dB, respectively. On the other hand, Ferdinandov et al and Kim Model (850 nm) at 2.3 km experience 11.29 dB and 11.3 dB loss respectively. The results are given in table 4-10.

Table 4-10: Power Link Margin and Total Atmospheric Attenuation versus Link Length

Power Link Margin and Total Atmospheric Attenuation Versus Link Length						
Distance (km)	**Power Link Margin (M(L)) (dB)**	**Ferdinandov et al Model (850 nm)-Total Power Losses (dB)**	**Kim Model (850 nm) - Total Power Losses (dB)**	**Ferdinandov et al Model (950 nm)-Total Power Losses (dB)**	**Kim Model (950 nm) - Total Power Losses (dB)**	**Kim Model (1550 nm) - Total Power Losses (dB)**
0.50	26.02	3.14215	3.16756	2.92266	2.95018	2.16804
1.00	20	5.95747	6.00829	5.53902	5.59407	4.10587
1.50	16.48	8.6623	8.73853	8.05183	8.13441	5.96587
2.00	13.98	11.29799	11.39963	10.49985	10.60995	7.77718
2.50	12.04	13.88355	14.0106	12.90089	13.03851	9.55317
3.00	10.46	16.42992	16.58238	15.26519	15.43034	11.30155
3.50	9.12	18.94419	19.12206	17.59942	17.79209	13.02733
4.00	7.96	21.43133	21.63461	19.90822	20.12842	14.73401
4.50	6.94	23.89503	24.12372	22.19505	22.44278	16.42417
5.00	6.02	26.33811	26.59221	24.46256	24.73781	18.0998
5.50	5.19	28.7628	29.04231	26.71282	27.0156	19.76247
6.00	4.44	31.1709	31.47582	28.94755	29.27785	21.41347
6.50	3.74	33.56391	33.89424	31.16814	31.52596	23.05384
7.00	3.1	35.9431	36.29884	33.37576	33.76111	24.68447
7.50	2.5	38.30952	38.69067	35.57142	35.9843	26.30611
8.00	1.94	40.6641	41.07066	37.75599	38.19639	27.9194
8.50	1.41	43.00764	43.43961	39.93021	40.39813	29.52493
9.00	0.92	45.34084	45.79822	42.09474	42.59019	31.12316
9.50	0.45	47.66432	48.14711	44.25016	44.77314	32.71456
10.00	0	49.97864	50.48684	46.397	46.9475	34.2995
10.50	-0.42	52.28429	52.8179	48.53571	49.11374	35.87833
11.00	-0.83	54.58173	55.14075	50.66672	51.27227	37.45138
11.50	-1.21	56.87134	57.45577	52.7904	53.42348	39.01892
12.00	-1.58	59.15351	59.76335	54.9071	55.5677	40.58121
12.50	-1.94	61.42856	62.06381	57.01714	57.70527	42.13849
13.00	-2.28	63.69681	64.35747	59.1208	59.83645	43.69098
13.50	-2.61	65.95853	66.6446	61.21834	61.96152	45.23887
14.00	-2.92	68.214	68.92548	63.31002	64.08072	46.78236
14.50	-3.23	70.46345	71.20034	65.39606	66.19428	48.3216
15.00	-3.52	72.7071	73.4694	67.47667	68.30242	49.85676

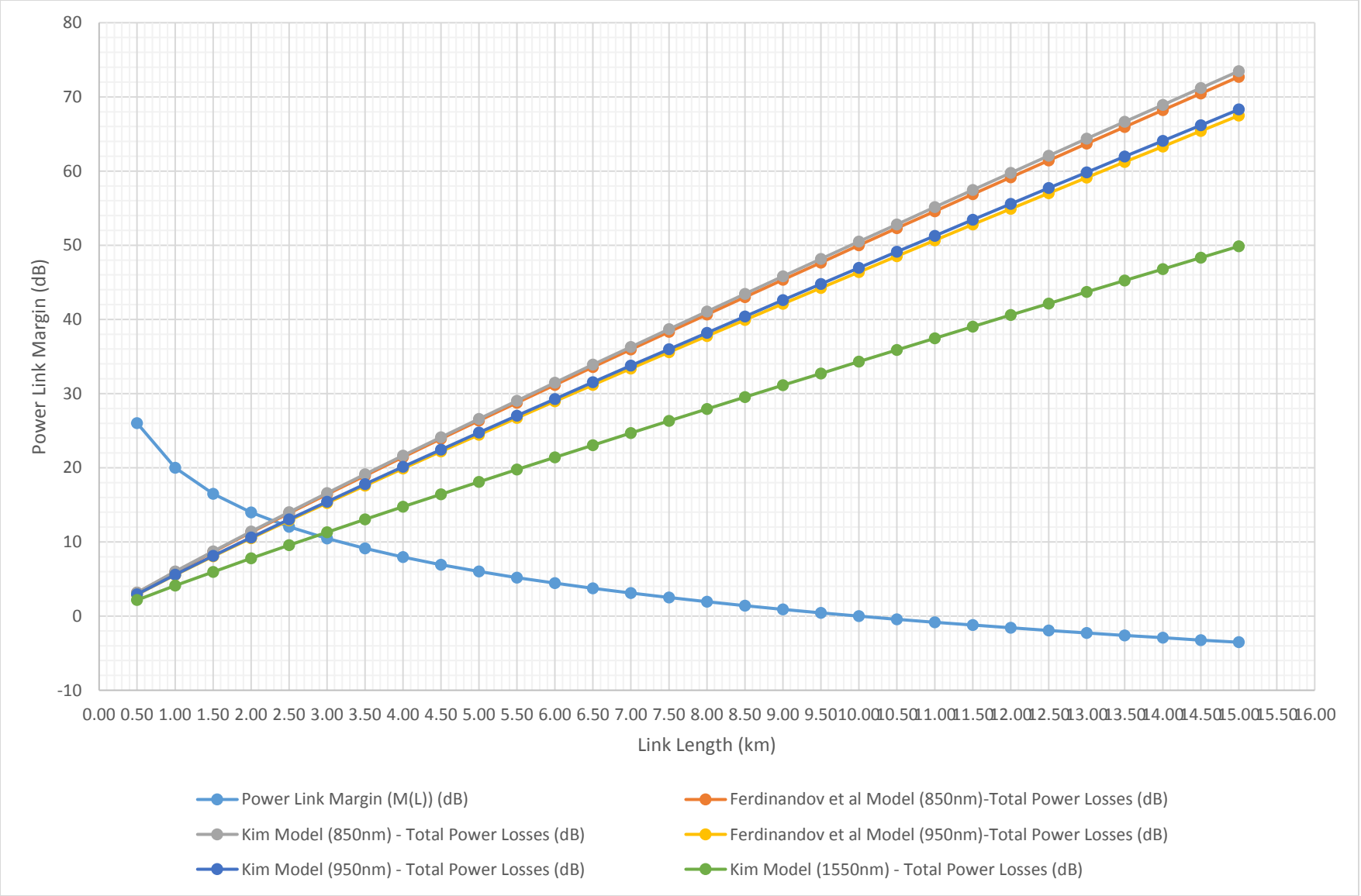

Figure 4-10: Power Link Margin and Total Atmospheric Attenuation against Link Length

Table 4-11: Power Scintillation Index at different refractive index

Power Scintillation Index ($m^{-2/3}$)									
	3.20711E-15			9.98883E-15			1.65591E-14		
Distance (km)	FSO A - 850 nm	FSO A – 950 nm	FSO A – 1550 nm	FSO B – 850 nm	FSO B – 950 nm	FSO B – 1550 nm	FSO C – 850 nm	FSO C – 950 nm	FSO C – 1550 nm
0.00	0.00000	0.00000	0.00000	0.00000	0.00000	0.00000	0.00000	0.00000	0.00000
0.50	0.00031	0.00031	0.00029	0.00096	0.00095	0.00091	0.00160	0.00158	0.00151
1.00	0.00231	0.00228	0.00210	0.00720	0.00709	0.00655	0.01193	0.01176	0.01085
1.50	0.00735	0.00721	0.00648	0.02289	0.02245	0.02019	0.03795	0.03722	0.03347
2.00	0.01651	0.01612	0.01418	0.05142	0.05021	0.04415	0.08525	0.08324	0.07320
2.50	0.03068	0.02984	0.02574	0.09556	0.09295	0.08017	0.15842	0.15409	0.13290
3.00	0.05061	0.04906	0.04159	0.15763	0.15280	0.12954	0.26132	0.25330	0.21474
3.50	0.07693	0.07433	0.06205	0.23960	0.23152	0.19327	0.39719	0.38381	0.32039
4.00	0.11017	0.10615	0.08738	0.34313	0.33061	0.27215	0.56882	0.54807	0.45116
4.50	0.15079	0.14491	0.11777	0.46966	0.45132	0.36682	0.77858	0.74818	0.60810
5.00	0.19920	0.19096	0.15340	0.62044	0.59475	0.47777	1.02854	0.98595	0.79203
5.50	0.25575	0.24459	0.19438	0.79654	0.76181	0.60541	1.32048	1.26290	1.00363
6.00	0.32072	0.30608	0.24082	0.99891	0.95331	0.75006	1.65596	1.58035	1.24343
6.50	0.39439	0.37563	0.29281	1.22837	1.16993	0.91199	2.03635	1.93947	1.51186
7.00	0.47700	0.45344	0.35042	1.48565	1.41229	1.09141	2.46285	2.34125	1.80929
7.50	0.56874	0.53969	0.41369	1.77138	1.68091	1.28848	2.93652	2.78655	2.13599
8.00	0.66979	0.63451	0.48268	2.08612	1.97624	1.50335	3.45830	3.27614	2.49220
8.50	0.78032	0.73804	0.55742	2.43039	2.29869	1.73613	4.02901	3.81069	2.87809
9.00	0.90048	0.85039	0.63793	2.80461	2.64861	1.98690	4.64938	4.39077	3.29381
9.50	1.03037	0.97166	0.72425	3.20919	3.02631	2.25574	5.32007	5.01690	3.73947
10.00	1.17013	1.10193	0.81638	3.64447	3.43206	2.54268	6.04166	5.68954	4.21516
10.50	1.31984	1.24128	0.91434	4.11076	3.86609	2.84778	6.81466	6.40906	4.72094
11.00	1.47960	1.38979	1.01813	4.60834	4.32862	3.17105	7.63952	7.17582	5.25685
11.50	1.64948	1.54750	1.12776	5.13745	4.81983	3.51252	8.51667	7.99013	5.82292
12.00	1.82956	1.71447	1.24324	5.69832	5.33987	3.87219	9.44645	8.85224	6.41916
12.50	2.01989	1.89075	1.36456	6.29113	5.88890	4.25006	10.4292	9.76239	7.04558
13.00	2.22054	2.07637	1.49173	6.91607	6.46703	4.64612	11.4652	10.7207	7.70216
13.50	2.43155	2.27136	1.62473	7.57328	7.07436	5.06038	12.5547	11.7276	8.38890
14.00	2.65297	2.47577	1.76357	8.26291	7.71100	5.49281	13.6979	12.7829	9.10576
14.50	2.88483	2.68960	1.90824	8.98507	8.37701	5.94339	14.8951	13.8870	9.85272
15.00	3.12717	2.91290	2.05873	9.73986	9.07247	6.41211	16.1463	15.0400	10.6297

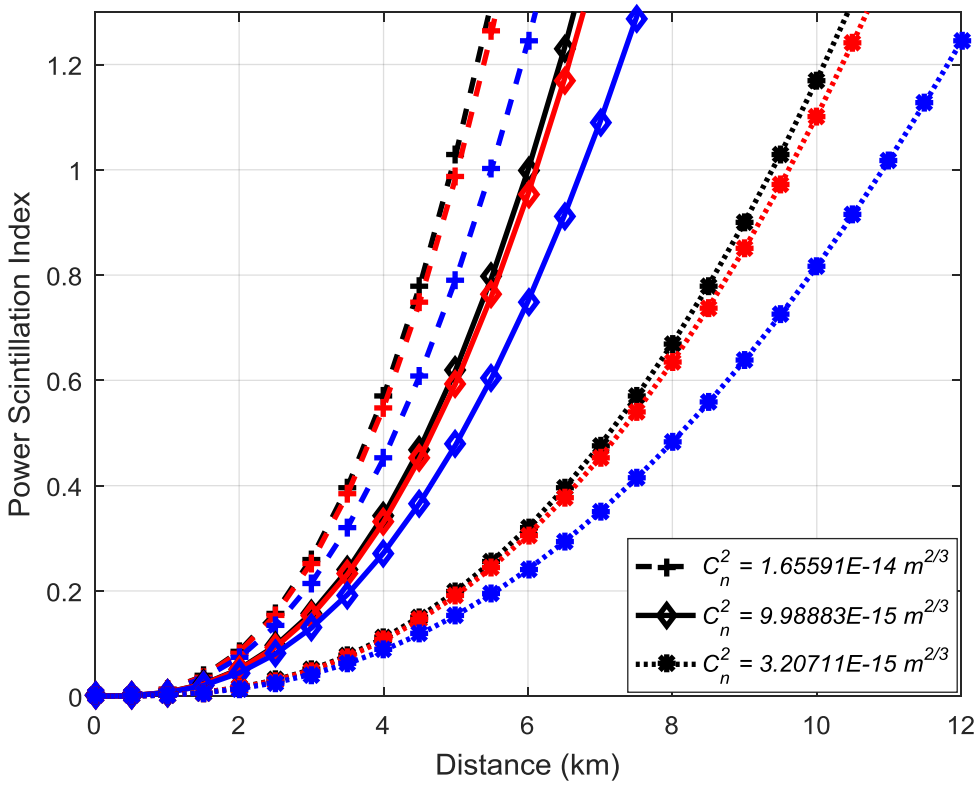

Figure 4-11: Power Scintillation Index at Receiver against Link Distance

Figure 4-11, shows the power scintillation index at different refractive indices. The influence of aperture averaging parameter on power scintillation index is also shown in Figure 4-11, where three refractive index parameters were employed for evaluation. The receiver aperture diameter can be seen in table 5-3. It is found that the effect of both the aperture diameter and refractive index parameter on the level of scintillation is comparatively large. It is observed that an increase in the diameter of the receiver aperture, results in a corresponding increase in the collector diameter. This results in the minimization of turbulence losses as the increased collector diameter allows merging of various optical intensities on the main component parts of the aperture lens. It is also noted that as the refractive index increases, it effects a corresponding increment in the power scintillation index at a specific link range. The results are given in table 4-11.

Table 4-12: Power Loss due to Turbulence (850 nm)

Power Loss due to Turbulence (850 nm)							
	Power S.I. ($m^{-2/3}$)	Atmospheric Turbulence (dB)					
Distance (km)	FSO B	$P_{ub} = 10^{-7}$	$P_{ub} = 10^{-4}$	$P_{ub} = 10^{-3}$	$P_{ub} = 10^{-2}$	$P_{ub} = 10^{-1}$	$P_{ub} = 2*10^{-1}$
0.00	0.00000	0.00000	0.00000	0.00000	0.00000	0.00000	0.00000
0.50	0.00096	0.70260	0.50316	0.41844	0.31552	0.17475	0.11548
1.00	0.00720	1.92793	1.38346	1.15219	0.87122	0.48694	0.32513
1.50	0.02289	3.44648	2.47922	2.06836	1.56923	0.88654	0.59908
2.00	0.05142	5.16537	3.72572	3.11422	2.37132	1.35523	0.92739
2.50	0.09556	7.01990	5.07767	4.25268	3.25044	1.87963	1.30242
3.00	0.15763	8.95699	6.49731	5.45253	4.18328	2.44726	1.71628
3.50	0.23960	10.93131	7.95181	6.68623	5.14873	3.04583	2.16037
4.00	0.34313	12.90490	9.41309	7.92990	6.12803	3.66354	2.62582
4.50	0.46966	14.84744	10.85822	9.16375	7.10521	4.28965	3.10411
5.00	0.62044	16.73623	12.26963	10.37238	8.06750	4.91501	3.58760
5.50	0.79654	18.55564	13.63481	11.54463	9.00535	5.53228	4.06987
6.00	0.99891	20.29603	14.94568	12.67305	9.91213	6.13590	4.54586

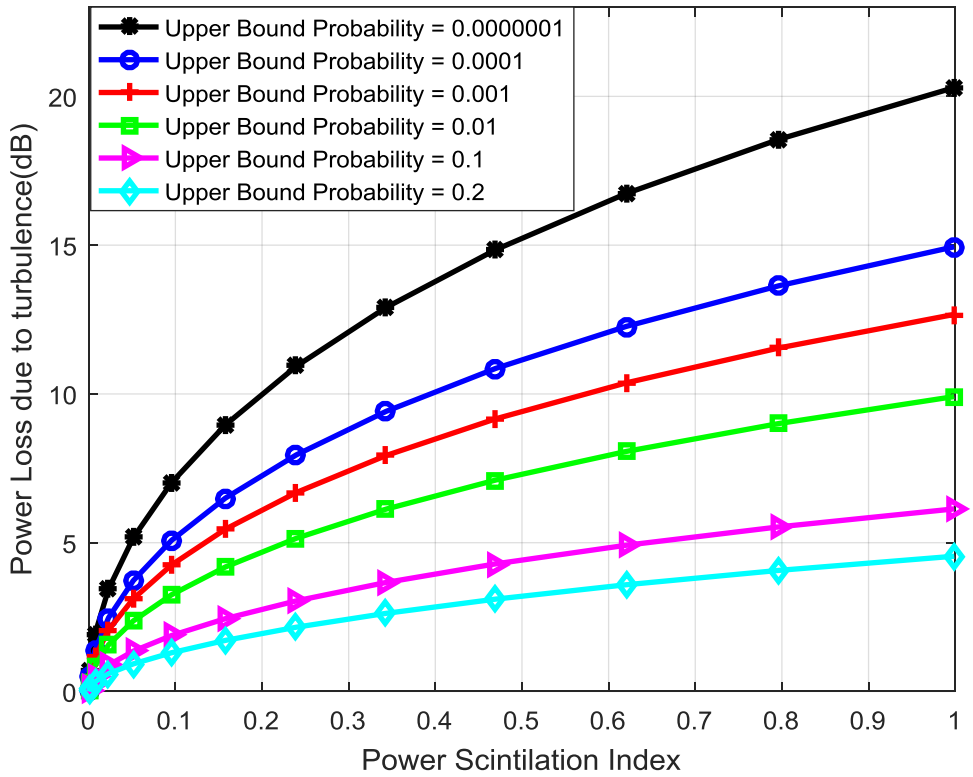

Figure 4-12: Power loss caused by turbulence plotted for differing upper bound at 850 nm

Table 4-13: Power Loss due to Turbulence (950 nm)

Power Loss due to Turbulence (950 nm)							
	Power S.I. ($m^{-2/3}$)	Atmospheric Turbulence (dB)					
Distance (km)	FSO B	$P_{ub} = 10^{-7}$	$P_{ub} = 10^{-4}$	$P_{ub} = 10^{-3}$	$P_{ub} = 10^{-2}$	$P_{ub} = 10^{-1}$	$P_{ub} = 2*10^{-1}$
0.00	0.00000	0.00000	0.00000	0.00000	0.00000	0.00000	0.00000
0.50	0.00095	0.69958	0.50099	0.41664	0.31416	0.17400	0.11498
1.00	0.00709	1.91388	1.37334	1.14374	0.86481	0.48331	0.32267
1.50	0.02245	3.41287	2.45491	2.04800	1.55367	0.87755	0.59285
2.00	0.05021	5.10435	3.68136	3.07693	2.34263	1.33830	0.91541
2.50	0.09295	6.92497	5.00829	4.19416	3.20510	1.85233	1.28272
3.00	0.15280	8.82350	6.39924	5.36951	4.11853	2.40751	1.68706
3.50	0.23152	10.75664	7.82283	6.57666	5.06273	2.99208	2.12019
4.00	0.33061	12.68832	9.25237	7.79292	6.01988	3.59483	2.57372
4.50	0.45132	14.58982	10.66618	8.99957	6.97487	4.20561	3.03956
5.00	0.59475	16.43963	12.04759	10.18202	7.91561	4.81576	3.51051
5.50	0.76181	18.22283	13.38469	11.32963	8.83302	5.41830	3.98047
6.00	0.95331	19.93016	14.66970	12.43526	9.72073	6.00796	4.44463

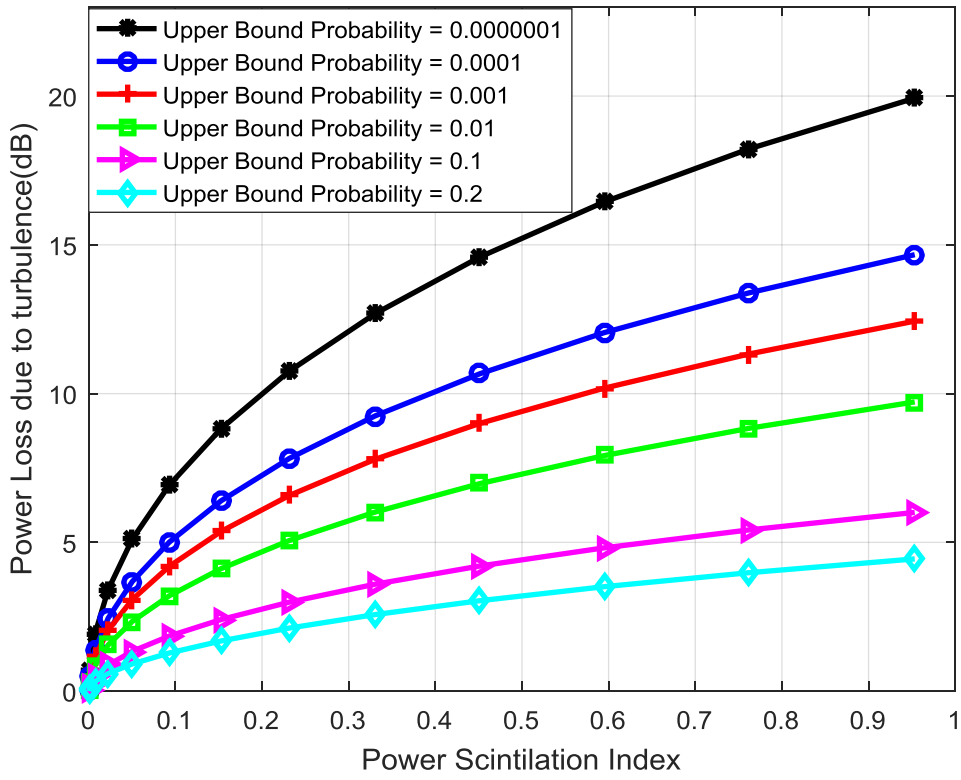

Figure 4-13: Power loss caused by turbulence plotted for differing upper bound at 950 nm

Table 4-14: Power Loss due to Turbulence (1550 nm)

Power Loss due to Turbulence (1550 nm)							
	Power S.I. ($m^{-2/3}$)	Atmospheric Turbulence (dB)					
Distance (km)	FSO B	$P_{ub} = 10^{-7}$	$P_{ub} = 10^{-4}$	$P_{ub} = 10^{-3}$	$P_{ub} = 10^{-2}$	$P_{ub} = 10^{-1}$	$P_{ub} = 2*10^{-1}$
0.00	0.00000	0.00000	0.00000	0.00000	0.00000	0.00000	0.00000
0.50	0.00091	0.68296	0.48908	0.40672	0.30667	0.16983	0.11221
1.00	0.00655	1.83838	1.31901	1.09839	0.83038	0.46381	0.30946
1.50	0.02019	3.23568	2.32680	1.94074	1.47173	0.83025	0.56014
2.00	0.04415	4.78748	3.45113	2.88350	2.19391	1.25073	0.85359
2.50	0.08017	6.43803	4.65271	3.89438	2.97311	1.71305	1.18248
3.00	0.12954	8.14524	5.90149	4.94843	3.79059	2.20697	1.54016
3.50	0.19327	9.87535	7.17295	6.02507	4.63056	2.72323	1.92011
4.00	0.27215	11.60112	8.44694	7.10717	5.47953	3.25334	2.31597
4.50	0.36682	13.30111	9.70730	8.18079	6.32629	3.78981	2.72178
5.00	0.47777	14.95918	10.94155	9.23501	7.16181	4.32620	3.13222
5.50	0.60541	16.56386	12.14057	10.26173	7.97919	4.85728	3.54274
6.00	0.75006	18.10767	13.29818	11.25529	8.77346	5.37897	3.94966

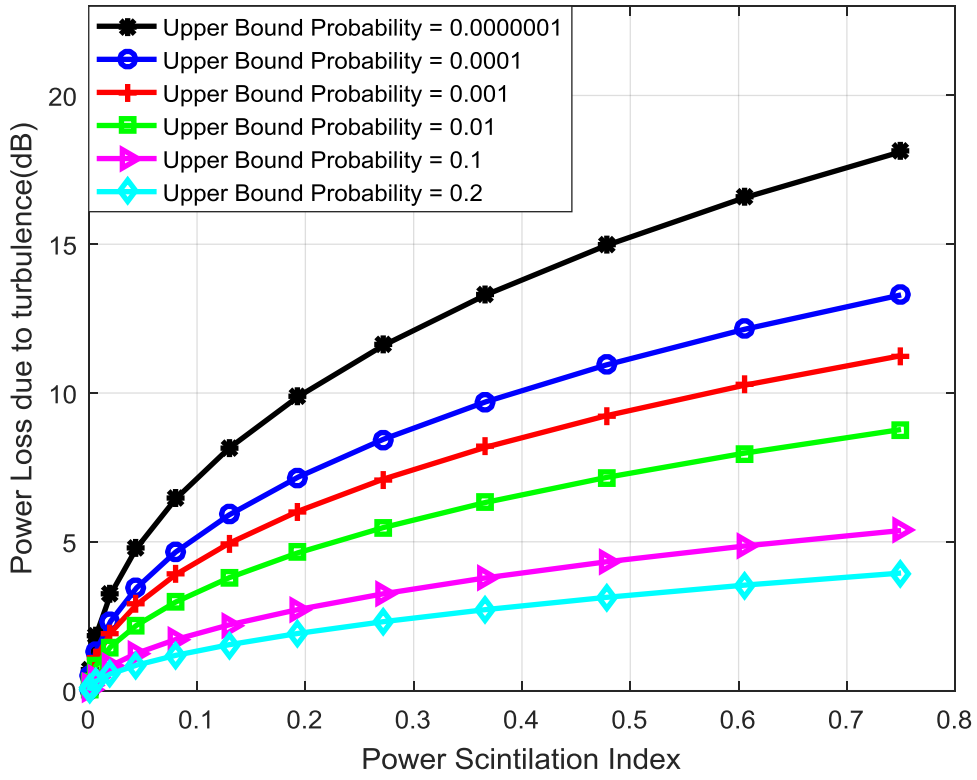

Figure 4-14: Power loss caused by turbulence plotted for differing upper bound at 1550 nm

Figure 4-12, 4-13 and 4-14 show that the power loss depends on the power scintillation index for different upper probabilities at 850 nm, 950 nm and 1550 nm wavelengths. It is noticed that the power loss due to turbulence effects increases as the power scintillation index increases. Hence, the necessary margin required for a specific FSO system bound probability must be assigned to compensate for the turbulence loss. The attenuation loss and the bound probability have a reciprocal relationship. Also, the turbulence loss increases with increase in the transmission link length. However, the wavelengths have minor or no influence on the attenuation loss properties but the fading loss depends strongly on the power scintillation index as observed in figure 4-12, 4-13 and 4-14 above. The results are given in Table 4-12, 4-13 and 4-14.

4.4 Probability of Exceeding Attenuation

We further evaluated the probability of exceeding atmospheric attenuations in the eastern coast of South Africa. Since visibility values are location dependent, atmospheric attenuation profiles also depends on geographical location. It is necessary to have an overview of the likely attenuation that might be encountered in a particular place per unit time before deployment of FSO systems. The methodological approach of probability of exceeding a specific attenuation in dB/km can be adopted to predict the FSO system outage probability for maximum possible atmospheric attenuation that it can encounter during optical signals propagation. The results are given in table 4-15.

Table 4-15: Probability of exceeding different Attenuation Values

Probability of exceeding different Attenuation Values					
Attenuation Values (dB/km)	**Kim Model – 850 nm**	**Fedinandov et al Model – 850 nm**	**Kim Model – 950 nm**	**Fedinandov et al Model – 950 nm**	**Kim Model – 1550 nm**
0.1	0.972222	1	0.967593	1	0.796296
0.2	0.958333	1	0.888889	1	0.638889
0.3	0.884259	1	0.800926	0.99537	0.037037
0.4	0.847222	0.75463	0.5	0.314815	0.037037
0.5	0.282407	0.25463	0.069444	0.111111	0.037037
0.6	0.069444	0.092593	0.037037	0.027778	0.037037
0.8	0.032407	0.023148	0.037037	0.013889	0.027778
1	0.032407	0.013889	0.032407	0.013889	0.023148
1.2	0.018519	0.013889	0.009259	0.013889	0.009259

Figure 4-15 shows the probability of encountering and exceeding different atmospheric fading conditions for 850 nm, 950 nm and 1550 nm wavelengths. Considering Kim model (850 nm), the probability of experiencing attenuation exceeding 0.1 dB/km is 0.972222 while the probability of encountering

probability exceeding 0.5 dB/km is 0.282407 and the probability of encountering attenuation exceeding or equal to the highest recorded attenuation for the eastern coast of South Africa that is 1.2 dB/km is 0.018519.

Using Ferdinandov model (850 nm), the probability of experiencing attenuation exceeding 0.1 dB/km is approximately 1 while the probability of encountering probability exceeding 0.5 dB/km is 0.25463 and the probability of encountering attenuation exceeding or equal to the highest recorded attenuation for the eastern coast of South Africa, that is, 1.2 dB/km is 0.013889.

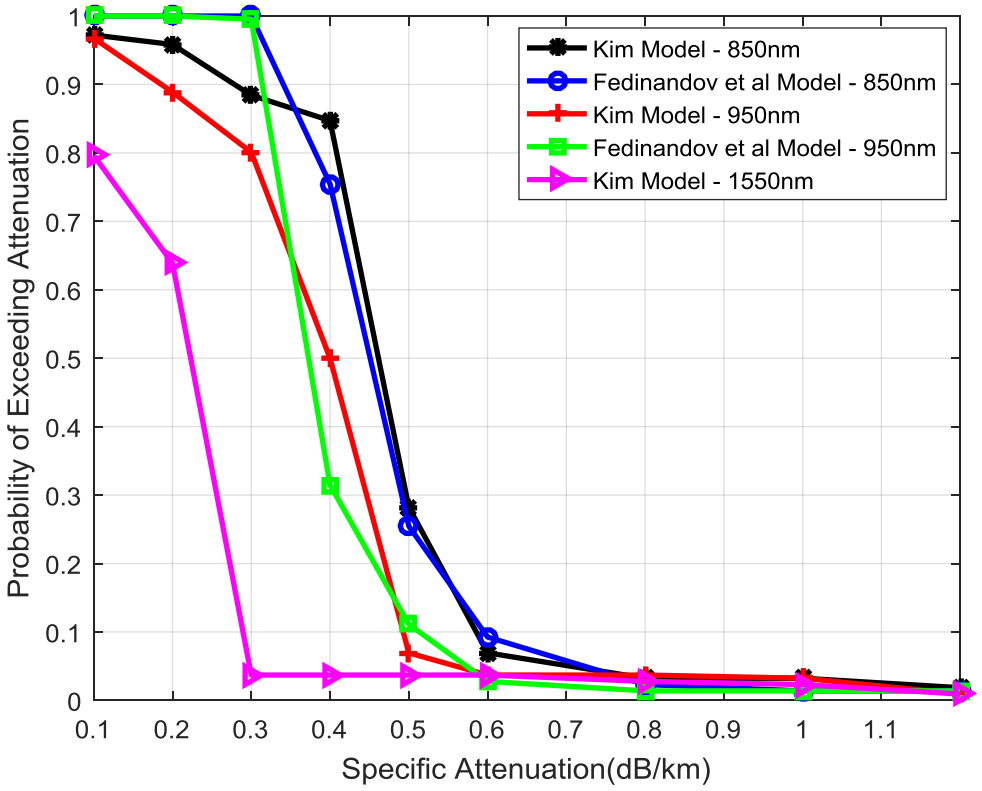

Figure 4-15: Probability of encountering different Atmospheric Attenuation Conditions

Using Kim model (950 nm), the probability of experiencing attenuation exceeding 0.1 dB/km is 0.967593 while the probability of encountering attenuation exceeding 0.5 dB/km is 0.069444 and the probability of encountering attenuation exceeding or equal the highest recorded attenuation for the eastern coast of South Africa, that is, 1.2 dB/km is 0.009259.

Using Ferdinandov model (950 nm), the probability of experiencing attenuation exceeding 0.1 dB/km is approximately 1 while the probability of encountering probability exceeding 0.5 dB/km is 0.111111 and the probability of encountering attenuation exceeding or equal the highest recorded attenuation for the eastern coast of South Africa, that is, 1.2 dB/km is 0.013889.

Using Kim model (1550 nm), the probability of experiencing attenuation exceeding 0.1 dB/km is 0.796296 while the probability of encountering probability exceeding 0.5 dB/km is 0.037037 and the probability of encountering attenuation exceeding or equal the highest attenuation for the eastern coast of South Africa, that is, 1.2 dB/km is 0.009259.

4.5 FSO Link Budget Analysis

For an ideal economic FSO system whose parameters are described in table 3-3, the attainable link distance as a function of the link margin and sensitivity for different visibility values is shown in figure 4-16. With reference to the losses examined in chapter three of this dissertation, the optical power received (dBm) can therefore be derived from equations 3.7, 3.23, 3.25 and 3.26. Results shown in figure 4-16 are obtained from Kim model and the technical specifications of the FSO equipment. The FSO system parameters for link budget analysis are given in table 4-16.

Table 4-16: Typical link budget parameters

System Parameters	**Typical Value**
Transmit Optical Output	16 dBm
Receiver Sensitivity	-38 dBm
Beam Divergence Angle	2.8 mrad
Receiver Coupling Loss	3 dB
Aperture Diameter	160 mm
Wavelength	850 nm
Modulation	On/Off Keying

By making the link to work at 5 dB link margin under clear sky, a link range of approximately 3 km is achievable at the specified data rate; increasing the link margin decreases the link range to fall below 1.5 km. The link margin can be enhanced by raising the propagated optical power in order to increase the

attainable link range. Attention must be given to the eye and skin safety standards when increasing the propagated optical power. The results for link margin analysis are given in table 4-17.

Table 4-17: Kim Model- Link Margin for Different Wavelength at Link length of 20 km.

Kim Model- Link Margin for Different Wavelength			
	Link Margin (dB)		
Link Length (km)	**Wavelength (850 nm)**	**Wavelength (950 nm)**	**Wavelength (1550 nm)**
0.50	28.50703	28.60465	28.86938
1.00	20.98409	21.27936	22.12879
1.50	15.28757	15.85018	17.52793
2.00	10.13851	10.98863	13.63974
2.50	5.35905	6.44921	10.05944
3.00	1.02251	2.26729	6.66126
3.50	0.00000	0.00000	3.43261
4.00	0.00000	0.00000	0.401

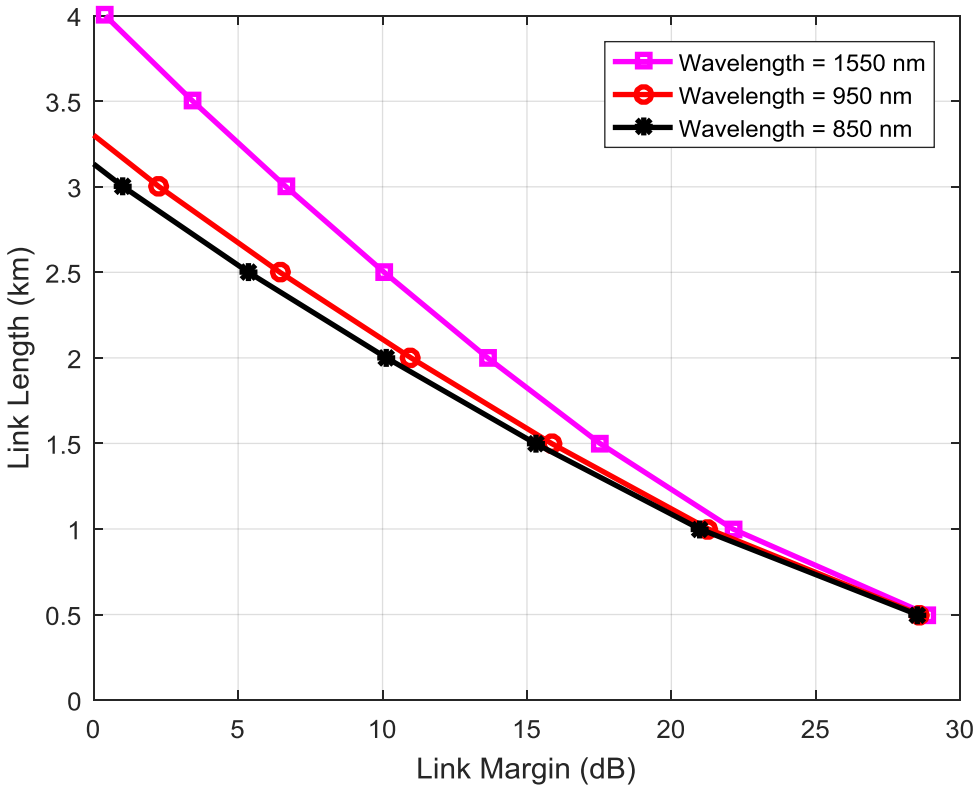

Figure 4-16: Link Length versus Link Margin for different values of wavelength at average visibility of 20 km.

Figure 4-16 shows the power link margin required to obtain a specific link length for various optical wavelengths at an average visibility of 20 km. A link margin of 10 dB would be needed to achieve approximate link distance values of 2.0 km, 2.1 km and 2.5 km on transmitting wavelengths of 850 nm, 950 nm and 1550 nm respectively. This indicates that greater link length is achieved on the 1550 nm wavelength as compared to the 850 nm and 950 nm optical wavelengths for a specific power link margin value. Propagation distances greater than 3.1 km, 3.3 km and 4.0 km on respective transmitting wavelengths of 850 nm, 950 nm and 1550 nm require a link margin below zero. This shows that the received signal power is lesser than the receiver sensitivity at such distances.

In order to achieve a reliable and consistent FSO link connection, the link margin must be equal to or higher than the overall atmospheric attenuation due to scattering and scintillation. The maximum link distance is reached at the points where the power link margin cut across the overall atmospheric attenuation lines for the respective optical field wavelengths (see figure 4-10). The maximum link range is reached for Kim model with 1550 nm wavelength at link length of 3 km, followed by Ferdinandov et al and Kim Model (950 nm) both at 2.5 km. On the other hand, Ferdinandov et al and Kim Model (850 nm) attained optimal link length at 2.3 km.

Minimum Required Visibility for FSO system

For consistent and reliable operation of FSO network, estimation of minimum required visibility is necessary. It helps to compute and examine the availability of an FSO link. For an FSO link to be available and reliable, the maximum FSO link distance and mean visibility value must be higher than the proportionate required minimum visibility. Figure 4-19 shows the minimum required visibility for reliable operation of an FSO system for different values of wavelength that is 850 nm, 950 nm and 1550 nm. It is observed that the minimum required visibilities for reliable operation of FSO systems increases as the link distance increases. Therefore, the minimum required visibilities for effective FSO operation is dependent on the link range. The results are given in table 4-20.

Table 4-18: Minimum Required Visibility for eastern coast of South Africa

Minimum Required Visibility (km)				
Link Margin (dB)	**Distance (km)**	**FSO A (850 nm)**	**FSO B (950 nm)**	**FSO C (1550 nm)**
30.02	0.50	0.16068	0.13905	0.07358
24.00	1.00	0.40198	0.34786	0.18408
20.48	1.50	0.70666	0.61153	0.32361
17.98	2.00	1.07317	0.92869	0.49145
16.04	2.50	1.50354	1.30113	0.68854
14.46	3.00	2.00188	1.73238	0.91675
13.12	3.50	2.57390	2.22739	1.17871
11.96	4.00	3.22690	2.79247	1.47774
10.94	4.50	3.96987	3.43542	1.81798
10.02	5.00	4.81381	4.16575	2.20446
9.19	5.50	5.77205	4.99498	2.64328
8.44	6.00	6.86084	5.93719	3.14189
7.74	6.50	8.10005	7.00958	3.70938
7.10	7.00	9.51420	8.23334	4.35698
6.50	7.50	11.13377	9.63488	5.09866
5.94	8.00	12.99714	11.24739	5.95198
5.41	8.50	15.15319	13.11318	6.93933
4.92	9.00	17.66519	15.28700	8.08969
4.45	9.50	20.61640	17.84090	9.44118
4.00	10.00	24.11863	20.87164	11.04501
3.58	10.50	28.32555	24.51220	12.97155
3.17	11.00	33.45431	28.95050	15.32024
2.79	11.50	39.82196	34.46089	18.23627
2.42	12.00	47.91037	41.46039	21.94032
2.06	12.50	58.48926	50.61509	26.78487
1.72	13.00	72.86879	63.05876	33.36990
1.39	13.50	93.47470	80.89058	42.80628
1.08	14.00	125.35678	108.48052	57.40652
0.77	14.50	181.05205	156.67776	82.91189
0.48	15.00	302.63361	261.89130	138.58957

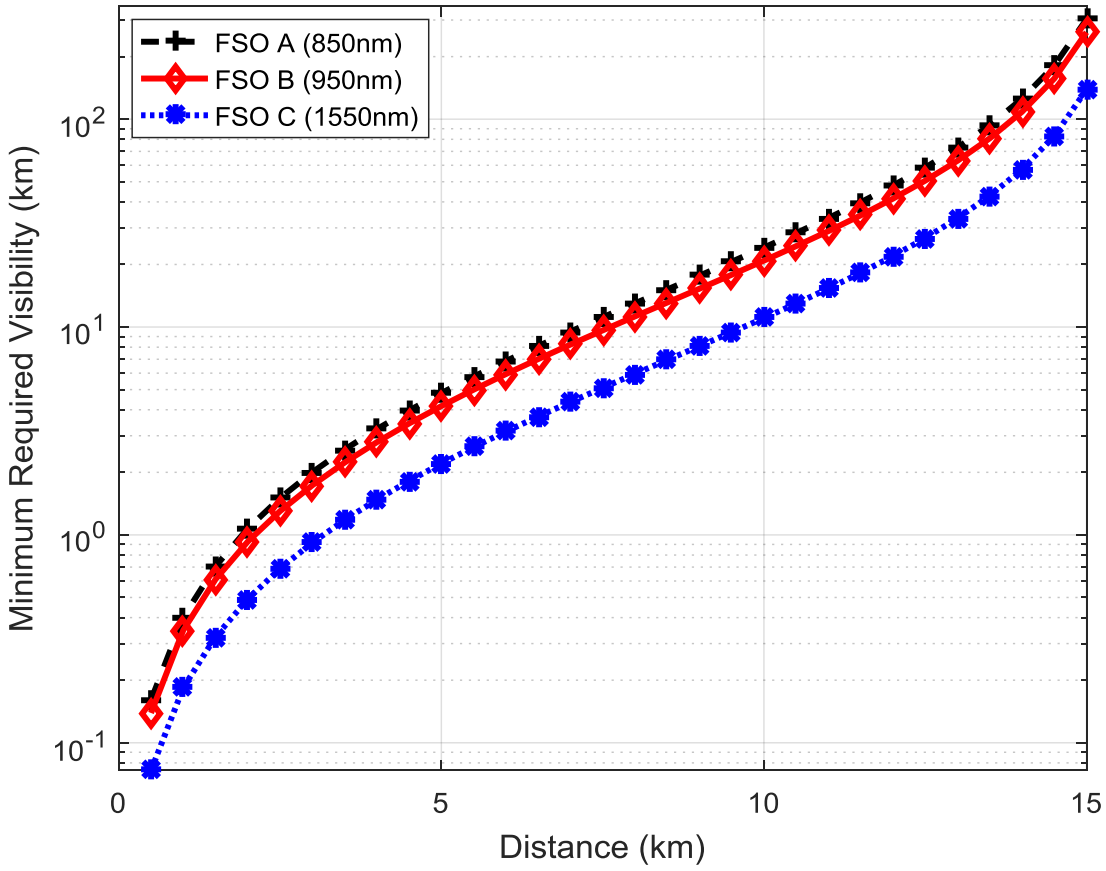

Figure 4-17: Minimum required visibility for accurate FSO system operation

4.6 FSO Link Availability

The FSO link availability strongly depends on the atmospheric attenuation parameters and the power link margin, which must be equal or higher than the overall atmospheric attenuation for a specific link distance. Figure 4-20 shows the dependence of FSO link availability on transmission link length and wavelengths. It is observed that the optical fields being propagated at 1550 nm wavelength provide better link availability over a particular link length compared to 850 nm and 950 nm wavelengths employed in this research work. The FSO link availability results for the eastern coast of South Africa at various link lengths are listed in Table 4-21. However, it is observed that he FSO link reliability and availability decreases as the transmission link length increases.

Table 4-19: FSO System Availability Estimation for eastern coast of South Africa

FSO System Availability Estimation			
Link Availability (%)			
Link Length (km)	**(850 nm)**	**(950 nm)**	**(1550 nm)**
1	100	100	100
2	100	100	100
3	100	100	100
4	100	100	100
5	98.6111	100	100
6	97.2222	98.1481	100

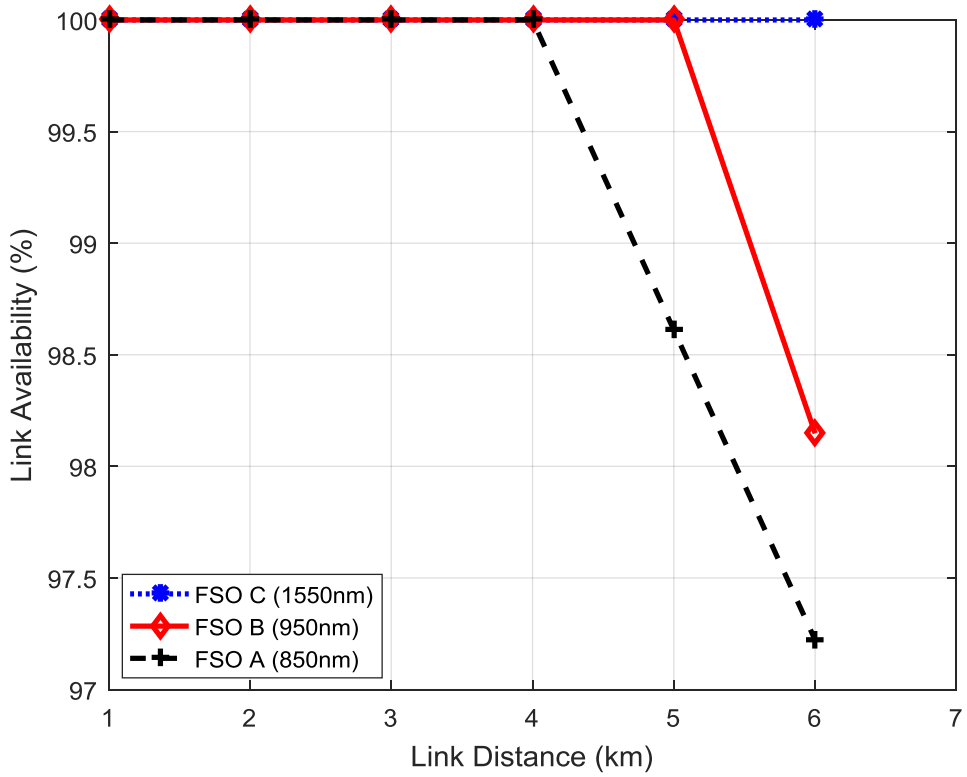

Figure 4-18: Link Availability for eastern coast of South Africa

4.7 Summary

In this chapter, the visibilities pattern, from which the atmospheric attenuation coefficients of the physical layer FSO systems were evaluated and presented for the eastern coast of South Africa. Power loss due to scattering and scintillation has been evaluated. The link margin to compensate for losses caused by scintillation impacts is discussed. It is observed that optimal link lengths occurs at the point where the power link margin intersects the corresponding average scattering atmospheric loss line. The probability of encountering and exceeding atmospheric attenuation was investigated. It is observed that using Kim model (850 nm), the probability of experiencing attenuation exceeding 0.1 dB/km is 0.972222 while the probability of encountering probability exceeding 0.5 dB/km is 0.282407 and the probability of encountering attenuation exceeding or equal to the highest recorded attenuation for the eastern coast of South Africa that is 1.2 dB/km is 0.018519. The FSO link budget and link availability are determined for the eastern coast of South Africa. The dependence of FSO link availability on transmission link length and wavelengths was examined. It is observed that the optical fields being propagated at 1550 nm wavelength provide better link availability over a particular link length compared to 850 nm and 950 nm wavelengths employed in this research work. However, the FSO system availability reduces with an increase in the propagation link distance.

Chapter 5 – Applications

5.1 Introduction

This chapter evaluates the performance of OFDM system mitigated by M-DPSK over an FSO atmospheric channel. Comparison will made between the OFDM system in non-turbulence and in turbulence environment. The performance of the OFDM-FSO communication system over a Log-normal channel for MQAM and BPSK modulation schemes will also be evaluated. The BER versuss SNR analyses will be performed as well.

5.2 Performance Analysis of OFDM-FSO Communication Systems Using M-DPSK Modulation

The techniques of orthogonal frequency division multiplexing (OFDM) with M-DPSK under the impaired FSO channel is employed to mitigate the impact of the atmospheric turbulence on the channel. The aim is to enhance the link performance of an FSO system. This technique will improve the data rate, improve bandwidth accessibility, easy frequency domain equalization, and higher spectral and power efficiency. The simulation of the OFDM system mitigated with M-DPSK over an FSO channel shows improved performance in non-turbulence compared to turbulence environment. The BER values as a function of signal to noise ratio (SNR) are determined for (M-DPSK) for assessing their relative performances for both non-turbulence and turbulence environment [53].

In figure 5-1, the fundamental parts of an ideal OFDM system for FSO system are illustrated below. It also shows the block diagram of an ideal system configuration for OFDM M-DPSK modulated system under the influence of impaired FSO channel.

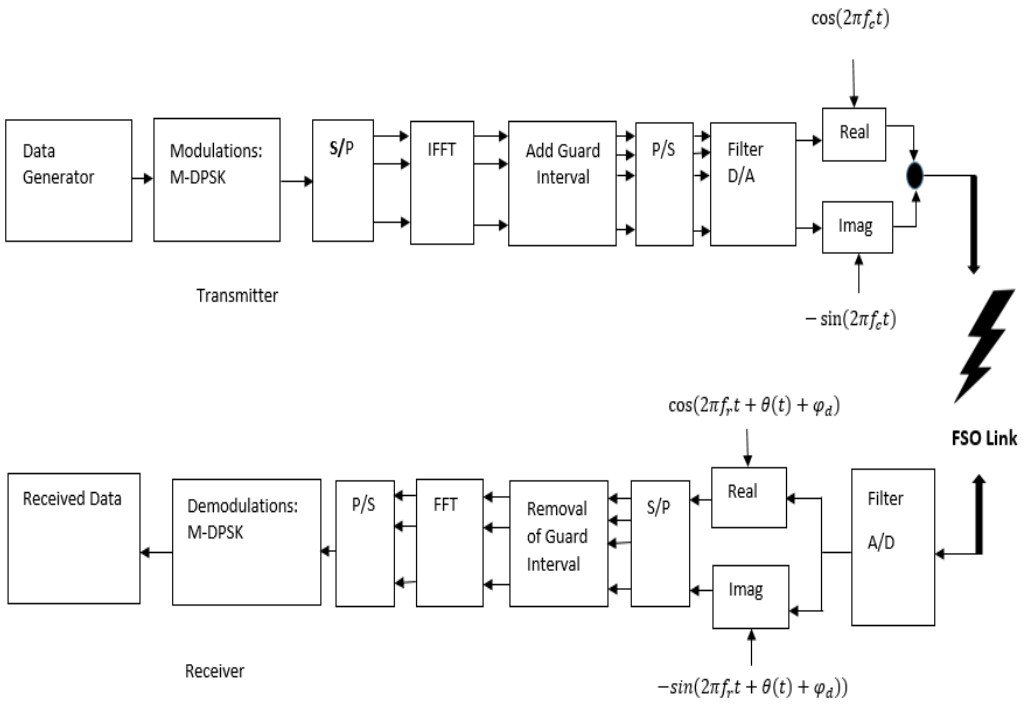

Figure 5-1: System configuration of OFDM-FSO communication system.

5.2.1 Non-Turbulence OFDM

The Non-turbulence OFDM can be expressed as [54].

$$Y_m = \frac{1}{\sqrt{L}} \sum_{a=0}^{L-1} x_a exp\left(\frac{-j2\pi ma}{L}\right) + \frac{1}{\sqrt{L}} \sum_{a=0}^{L-1} w_a exp\left(\frac{-j2\pi ma}{L}\right) \tag{5.1}$$

$$Y_m = X_m + W_m \tag{5.2}$$

where Y_m denotes the parameter of the noise of the mth optical output for the FFT Receiver, which enables optical signal to Noise Ratio (SNR) changes, x_a is the IFFT output data to be traversed on a subcarriers in time domain. X_m denotes the input data to be propagated on m subcarriers in the frequency domain, and L is the link length.

5.2.2 Turbulence OFDM

The turbulence OFDM can be expressed as [54]:

$$Y_m = \frac{1}{\sqrt{L}}\sum_{a=0}^{L-1} x_a exp\left(\frac{-j2\pi ma}{L}\right) \times T_m + \frac{1}{\sqrt{L}}\sum_{a=0}^{L-1} w_a exp\left(\frac{-j2\pi ma}{L}\right) \tag{5.3}$$

$$T_m = P(t)L_\alpha L_{Atm} L_{scin} \tag{5.4}$$

where $P(t)$ denotes the optical output power from the laser diode (LD) that is propagated through the atmosphere using an antenna, L_{scin} denotes losses due to scintillation, L_{Atm} denotes losses due to the atmosphere, such as rain and low-visibility fading losses and L_α denotes optical loss, geometrical loss, and pointing error losses [28].

$$Y_m = T_m X_m + W_m \tag{5.5}$$

where T_m denotes the OFDM-Turbulence link, W_m denotes the additive white Gaussian noise, X_m denotes the input data to be propagated on m subcarriers in the frequency domain, which the probability density function (pdf) is expressed as [55]:

$$p(I) = \frac{1}{\sqrt{2\pi\sigma_I}}\frac{1}{I} exp\left\{-\frac{(In(I/\langle I\rangle) + {\sigma_I}^2(D))^2}{2{\sigma_I}^2(D)}\right\} \tag{5.6}$$

where I denotes the irradiance at the receiver and $\langle I\rangle$ denotes the irradiance without scintillation. The range of the turbulence is represented by Rytov variance expressed as [55]:

$${\sigma_R}^2 = 1.23{C_r}^2 k^{7/6} L^{11/6} \tag{5.7}$$

where σ_R denotes the turbulence strength, $k = 2\pi/\lambda$ is the wave number, λ is wavelength, L denotes the link length and ${C_r}^2$ denotes the refractive index.

5.2.3 Comparative analysis of OFDM-FSO system performance

For a specific signal to noise ratio (SNR) value, the corresponding system bit error rate (BER) is observed. The results of the system performance for various arrays of differential phase shift keying (M-DPSK) modulation technique i.e. (4, 8, 16, 32 and 64-DPSK) for both non-turbulence and turbulence channel are presented. The BER values in terms of signal to noise ratio (E_b/N_o) are determined for (M-DPSK) by studying their relative performances for both non-turbulence and turbulence links.

Figure 5-2 shows the BER Performance of a non-turbulence channel for 4, 8, 16, 32 and 64-DPSK-OFDM. It can be noticed from figure 5-2 that the BER decreases exponentially as SNR (E_b/N_o) increases. It also reveals that the SNR of ~13 dB is achievable for a BER of ~10^{-5} for non-turbulence 4-DPSK-OFDM modulation.

Comparing the BER performances for the various M-DPSK, it is noticed that the use of a higher M-array DPSK as shown in figure 5-2, is better for high capacity transmission but the challenge occurs when the points of the constellation are closer which makes the propagation less robust to errors with same SNR.

Similarly, Figure 5-3 shows the BER performance of turbulence for 4, 8, 16, 32 and 64-DPSK-OFDM. It also reveals that the SNR of ~16 dB is attainable for a BER of ~10^{-6} for turbulence 4-DPSK-OFDM modulation. It is also noticed here that the BER decreases exponentially as SNR (E_b/N_o) increases. The constellation points for larger M-array DPSK under turbulence are shrinking and closer to each other which reduces the signal strength and makes the transmitted data more prone to errors for the same SNR.

Figure 5-4 shows the fluctuations in the BER Performance of non-turbulence and turbulence for 4, 8, 16, 32 and 64-DPSK-OFDM. It also shows the SNR variation for the OFDM transmission considering non-turbulence and turbulence for 4, 8, 16, 32 and 64-DPSK-OFDM modulation.

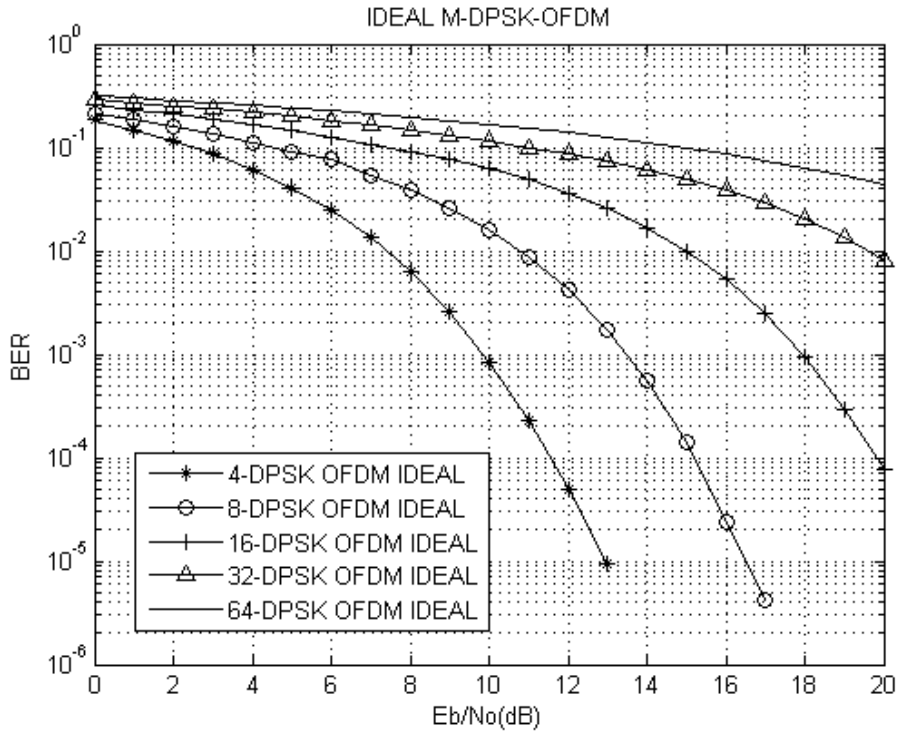

Figure 5-2: BER Performance Comparison of Non-Turbulence 4, 8, 16, 32 and 64-DPSK-OFDM

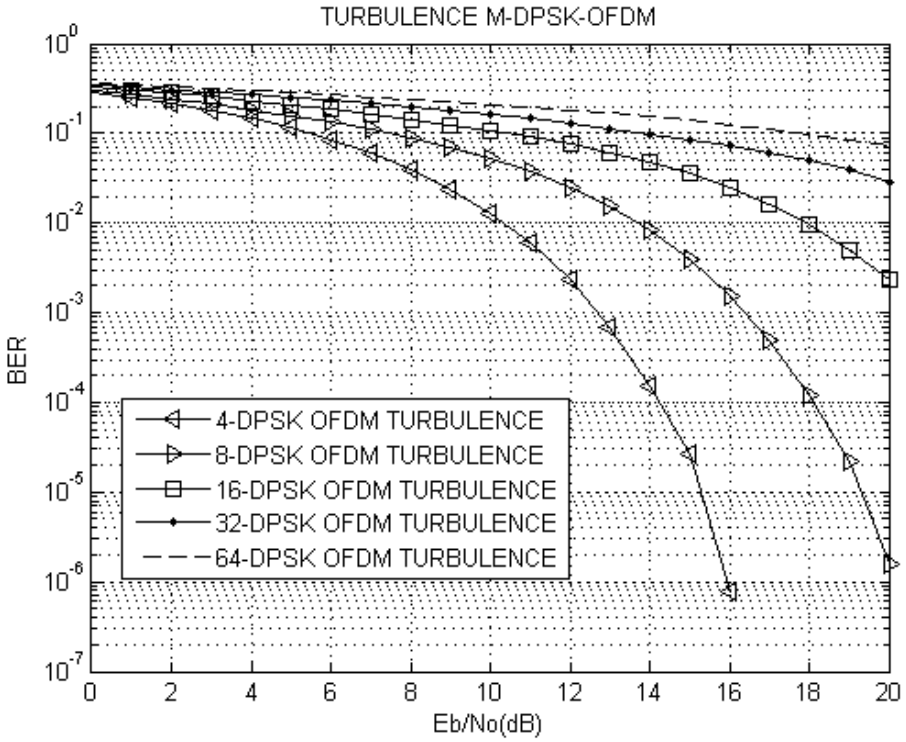

Figure 5-3: BER Performance Comparison of Turbulence 4, 8, 16, 32 and 64-DPSK-OFDM

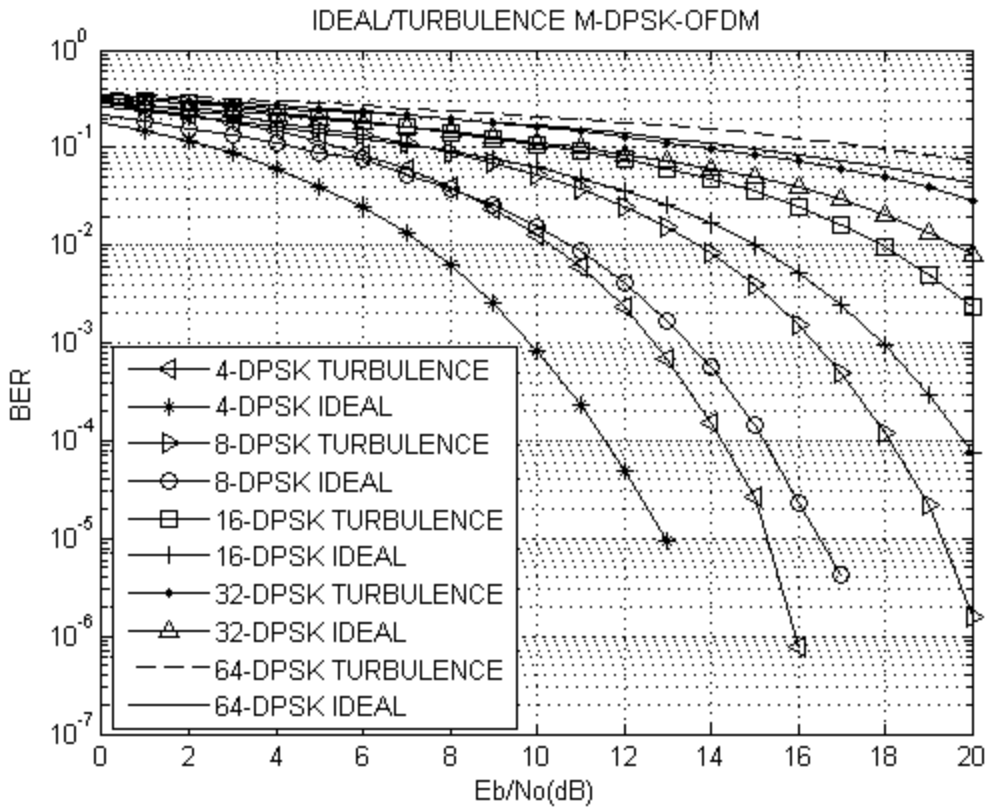

Figure 5-4: BER Performance Comparison of Non-turbulence/Turbulence for 4, 8, 16, 32 and 64-DPSK OFDM-FSO system.

Figure 5-4 shows that the BER vs SNR curve, at SNR of ~17 dB the BER of the system with OFDM is ~10^{-5} for non-turbulence 8-DPSK modulation and at SNR of ~20 dB, the BER of ~10^{-6} is achievable for turbulence using 8-DPSK modulation. During OFDM transmission, it is observed that, there is a reduction of ~10^{-1} in the BER, and a significant improvement of ~16 dB in SNR between non-turbulence 4-DPSK and turbulence 4-DPSK modulation. Similarly the SNR performance shows an improvement of ~20 dB for turbulence for 8-DPSK modulation in relation to non-turbulence 8-DPSK.

The BER against SNR results show that at a threshold BER value of ~10^{-5}, the SNR values attainable indicates a significant improvement of ~16 dB for 4-DPSK non-turbulence compared to 4-DPSK turbulence and ~20 dB for turbulence 8-DPSK modulation compared to non-turbulence 8-DPSK modulation. It also shows that increasing the modulation level causes an increase in the BER, which makes lower order M-DPSK modulation a preferred modulation for generation of OFDM signals when using M-DPSK modulation scheme under FSO channels.

5.3 Performance Evaluation of OFDM-FSO Communication Systems using *M*-QAM and BPSK Modulation under Log-Normal Channel

Orthogonal frequency division multiplexing (OFDM) is a promising modulation and multiplexing technique which is generally adopted in radio band wired and wireless technologies due to its various advantages like its ability to overcome multipath delay spreading of propagating signals, immunity to frequency selective attenuation and high spectral efficiency. Division of the frequency band of the spectrum into sub bands by allocating appropriate data streams to individual bands by OFDM can also enable the bandwidth and power efficiency of the propagating signals to increase. Due to its various advantages, IEEE 802.11a wireless local area network and IEEE 802.16 has now chosen OFDM modulation technique as their standards [56].

The performance of OFDM FSO channel with *M*-QAM and BPSK under the influence of atmospheric conditions are adopted to reduce the atmospheric attenuation and turbulence effects on the propagating signals. This mechanism will result in a new hybrid system called the OFDM-FSO system which will inherit the numerous advantages of both OFDM and FSO systems. Thus, it will optimize data rates of traversed signals over an FSO channel such as improved bandwidth access, easy and adequate deployment, simple frequency spectrum equalization, large spectral and power efficiency etc. making it an appropriate network for *last mile* solutions for broadband technology accessibility [55].

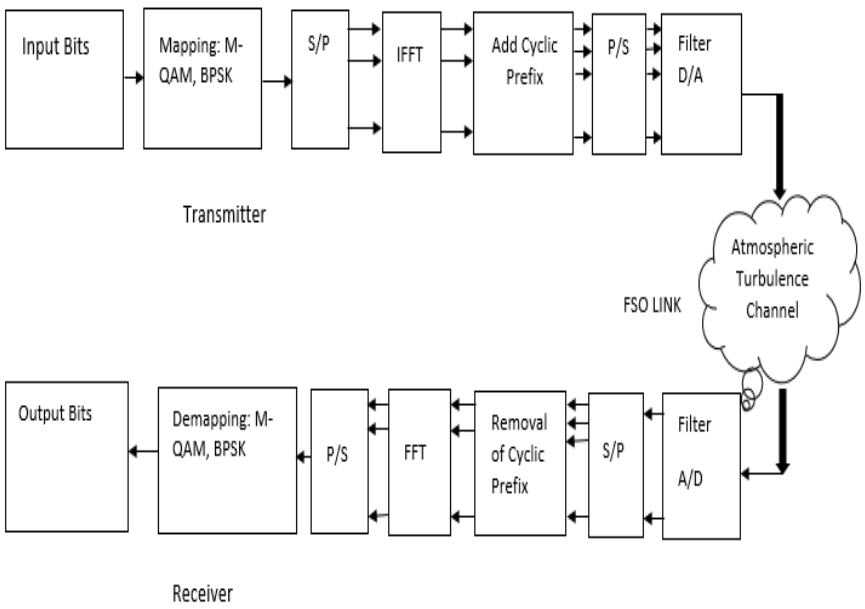

Figure 5-5: Schematic Diagram of OFDM-FSO System.

The resulting OFDM signal for N subcarriers, in wireless service carrier frequency f_c after up-conversion, may be expressed as [28]:

$$S_{ofdm}(t) = \sum_{n=0}^{N-1} s_n(t) \tag{5.8}$$

$$S_{ofdm}(t) = \frac{1}{\sqrt{T}} \sum_{0}^{K-1} a_k e^{\frac{j2\pi kt}{T}} \; w(nT) \tag{5.9}$$

where T represents the duration of OFDM symbol, a_k represents the bits of the signal and w(.) denotes the rectangular function. The optical power from the intensity of the laser after being linearly modulated by an OFDM signal with N subcarriers, can be expressed as [57]:

$$P_n(t) = P_{m(t)} \sum_{n=0}^{N-1} m_n s_n(t) \tag{5.10}$$

where $P_{m(t)}$ represents the mean propagated power, m_n denotes the optical modulation index (OMI) for individual subcarriers and the sum total OMI is expressed as [57]:

$$m_{(total)} = \frac{1}{N} \sqrt{\sum_{n=0}^{N-1} {m_n}^2} \tag{5.11}$$

The variation of the field at a specific period of time in the FSO link, may be expressed by multiplying both the stochastic amplitude and field attenuation of free space. The optical power received at the input of the photodiode may be expressed as [28]:

$$P_{rfso}(t) = P_n(t) L_\alpha L_{Atm} L_{scin} X_m \; + W_m \tag{5.12}$$

where $P_n(t)$ represents the laser diode output power transmitted over an optical wireless channel employing an antenna, L_{Atm} denotes losses due to the atmosphere, such as rain and low-visibility fading losses, L_{scin} denotes losses due to scintillation, L_α denotes losses like loss due to divergence of light beam, loss due to optical fiber, and loss due to pointing error effect. X_m measures the input data to be propagated on m

subcarriers in the frequency domain under the impact of atmospheric turbulence during propagation in FSO medium, its (pdf) is given by equation (34) and (35) [28].

5.3.1 Quadrature Amplitude Modulation

Quadrature Amplitude Modulation (QAM) is a type of band-pass digital modulation scheme used for conveying signals over long link distances. It provides a highly improved spectral efficiency when transmitting numerous bits for respective symbols through OFDM-FSO channel but with a defined power efficiency. In relation to the BPSK modulation schemes, QAM is immune to influence of inter-symbol interference (ISI), but very sensitive to non-linearity of the link and noise [58].

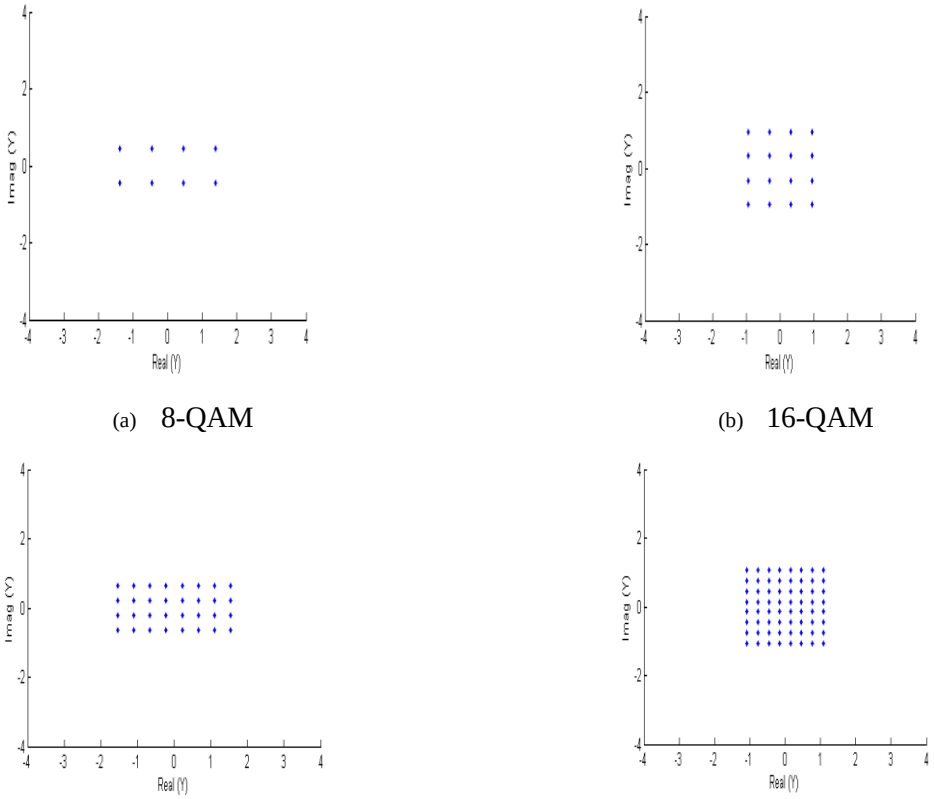

(a) 8-QAM (b) 16-QAM

(c) 32-QAM (d) 64-QAM

Figure 5-6: Transmitted Signal Constellations Graph of M-QAM for OFDM-FSO communication system under Log-normal channel.

Figure 5-6 shows the constellations of signals before undergoing modulation of different M-ary of Quadrature Amplitude modulation schemes; namely, 8-QAM, 16-QAM, 32-QAM and 64-QAM at the transmitting end of the OFDM-FSO communication network. The M-Ary modulations help to collect and arrange the input bits to form symbols, which are transmitted in the form of signals [59].

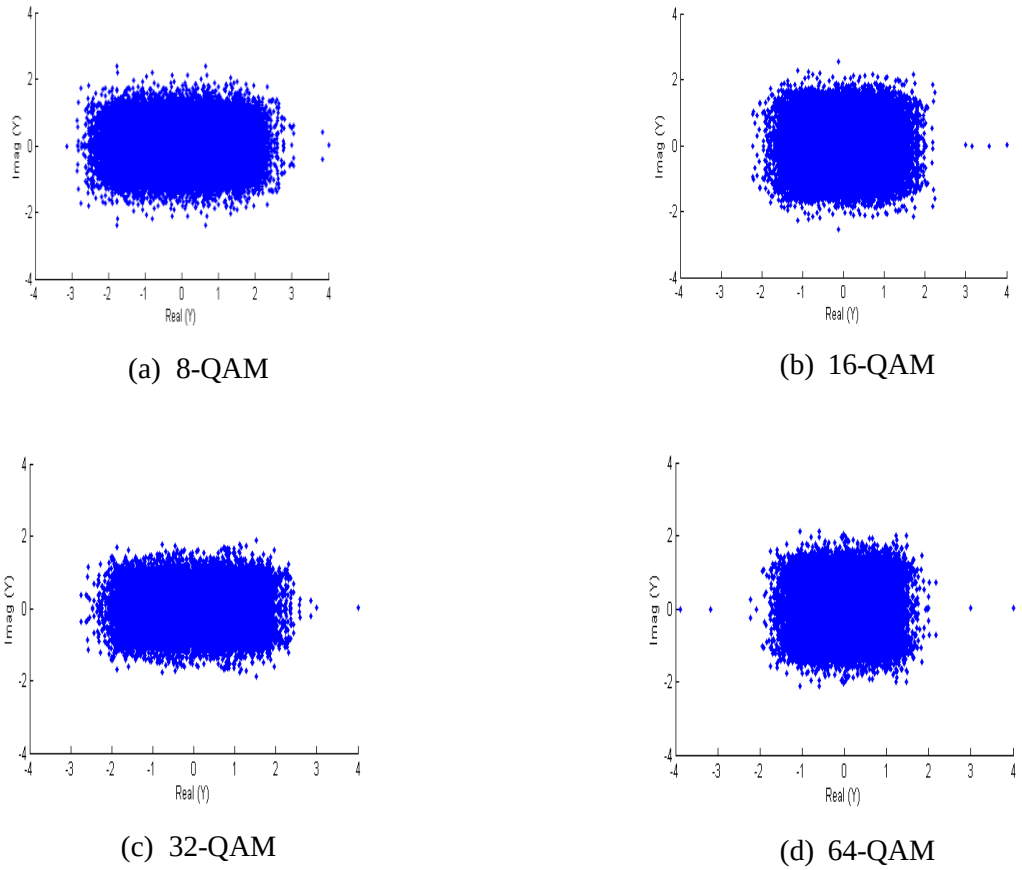

(a) 8-QAM

(b) 16-QAM

(c) 32-QAM

(d) 64-QAM

Figure 5-7: Received Signal Constellations Graph of M-QAM for OFDM-FSO communication system under Log-Normal Channel.

Figure 5-7 shows the constellations of signals after being modulated by various M-ary of Quadrature Amplitude modulation schemes; namely, 8-QAM, 16-QAM, 32-QAM and 64-QAM at the transmitting end of the OFDM-FSO communication network.

Figure 5-8 shows that with 8-QAM and 16-QAM modulation schemes, BER is relatively $\sim 10^{-2}$ at SNR of ~12 dB; however the SNR cannot be increased further as there would be no significant variation in the received BER value while for 32-QAM and 64-QAM, the resultant BER versus SNR curve shows that the received BER is relatively $\sim 10^{-1}$ at SNR of ~12 dB and a BER of 10^{-4} at ~12 dB is obtained for BPSK.

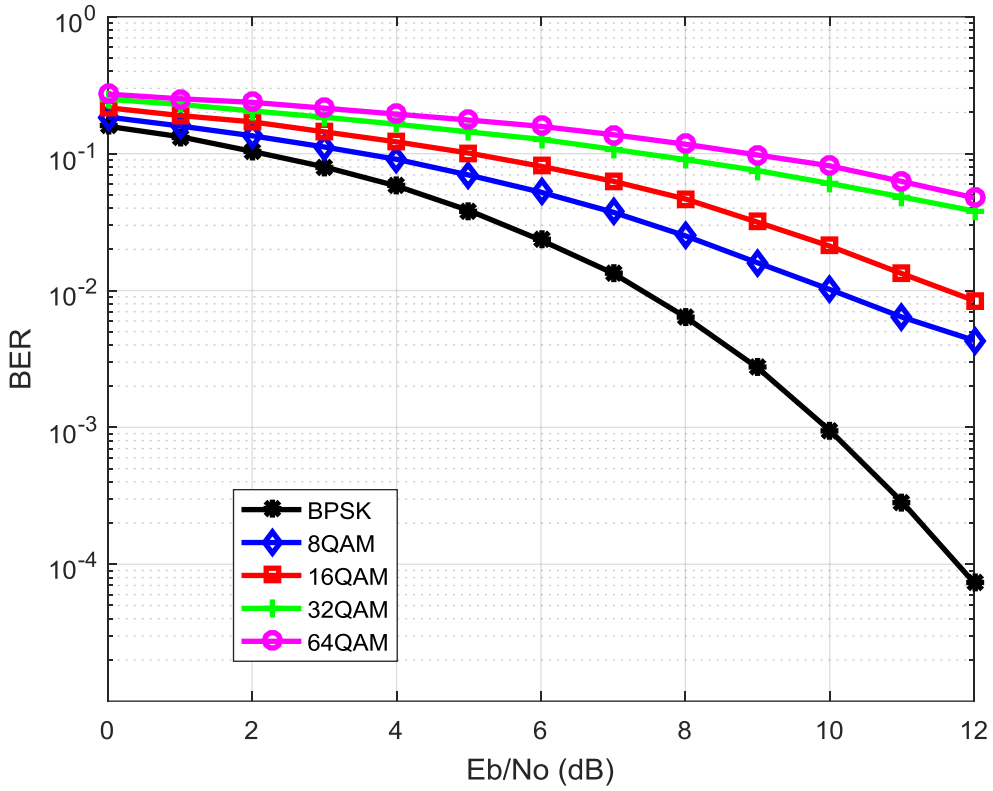

Figure 5-8: BER versus SNR curve for OFDM-FSO system under Log-normal channel with M-QAM and BPSK Schemes at ${\sigma_I}^2 = 0.5$.

It is also observed that BPSK has a good power efficiency. To obtain a lower BER and highly improved bandwidth, *M*-QAM modulation schemes will be adopted while BPSK is suitable when propagating optical signals at large power for better improved power efficiency.

Figure 5-9 shows that for the same values of SNR and wavelength of 850 nm, the BER of the system with the M-QAM and BPSK modulation schemes, increases as the link length increases. This implies that at various OFDM-FSO link distances, that is (L= 1 km, L= 3 km and L= 5 km), the effects of atmospheric attenuation and turbulence increases as the link distance increases. The system experiences poor performance with large values of link distance L and at larger value of SNR.

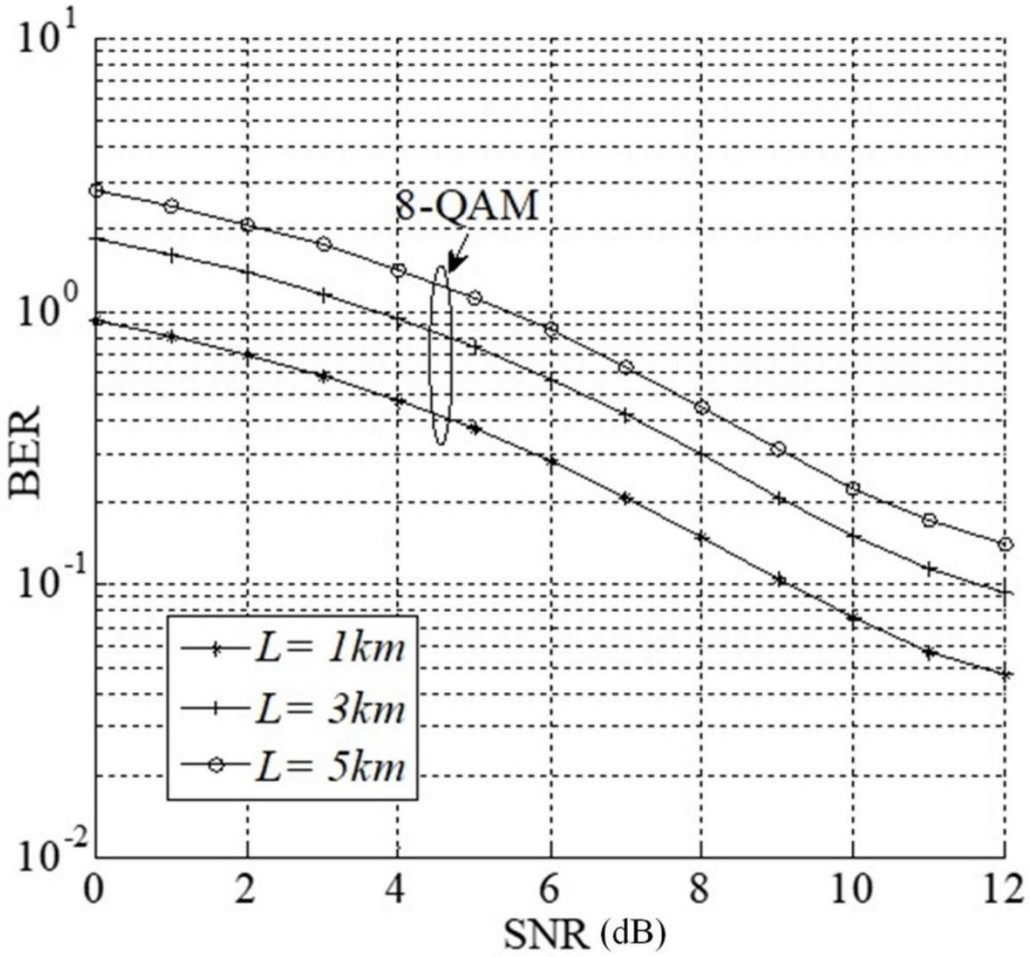

Figure 5-9: BER versus SNR curve for 8-QAM Scheme at different OFDM-FSO link lengths under Log-normal channel at λ= 850 nm.

The performance of OFDM-FSO communication system under Log-normal channel for various MQAM i.e. (8-QAM, 16-QAM, 32-QAM, 64 - QAM) and BPSK modulation schemes is analysed. The BER versus SNR analysis is performed. The results show that there is a reduction of approximately 10^{-4} in BER for BPSK compared to 8-QAM modulation scheme used over the OFDM-FSO Log-normal channel. It is also observed that for the 8-QAM modulation scheme for the same values of wavelength and SNR, BER increases with respect to an increase in the Log-normal channel length. The BER versus SNR analyses carried out also reveal that BPSK has a good power efficiency. In order to obtain a low BER, highly improved bandwidth, M-QAM modulation schemes should be considered while BPSK is suitable when transmitting at high power for better enhanced power efficiency.

5.4 Summary

This chapter examines the performance of an OFDM system mitigated by M-DPSK over free space optics channel, which shows that the OFDM system is improved in non-turbulence as compared to turbulence environment. The results shows that The BER against SNR results show that at a threshold BER value of ~10^{-5}, the SNR values attainable indicates a significant improvement of ~16 dB for 4-DPSK non-turbulence compared to 4-DPSK turbulence and ~20 dB for turbulence 8-DPSK modulation compared to non-turbulence 8-DPSK modulation. It also shows that increasing the modulation level causes an increase in the BER, which makes lower order M-DPSK modulation a preferred modulation for generation of OFDM signals when using M-DPSK modulation scheme under FSO channels.

The performance of OFDM-FSO communication system under Log-normal channel for MQAM i.e. (8-QAM, 16-QAM, 32-QAM, 64-QAM and BPSK) modulation schemes was also evaluated. The results show that there is a reduction of approximately 10^{-4} in BER for BPSK compared to 8-QAM modulation scheme used over the OFDM-FSO Log-normal channel. It is also observed that for 8-QAM modulation scheme for the same values of wavelength and SNR, BER increases with respect to an increase in the Log-normal channel length. The BER versus SNR analyses carried out reveal that, in order to obtain a low BER and highly improved bandwidth, M-QAM modulation schemes should be considered while BPSK is suitable when transmitting at high power for better enhanced power efficiency.

Chapter 6 - Conclusion and Future Work

6.1 Conclusion

The FSO system is now gaining momentum among researchers as a viable complementary for high/immense capacity network accessibility due to its numerous advantages such as high bandwidth, low power consumption, license-free frequency spectrum, simple and low cost of installation, small size etc. over its RF counterpart for various applications both indoor and outdoor. This dissertation is mainly aimed at investigating and evaluating the performance of FSO systems over weak atmospheric turbulence channels with the view to understand its feasibility, characteristics and limitations for the eastern coast of Southern Africa. Additionally, it also aimed to find techniques to mitigate the effect of atmospheric turbulence on the performance of FSO communication systems.

In order to achieve the aims and objectives of this research work, a background summary about the FSO system, history, properties, applications, system configuration, eye safety standards and terminologies were discussed in the chapter two. Optical detection processes and sources of noise at the receiver and their effects on the performance of FSO systems were also examined in the same chapter. With regards to the atmospheric channel, the atmospheric attenuation and scintillation were also analyzed.

Chapter Three examined and discussed the various statistical models used in this dissertation. These include models for estimating the diverse losses encountered by optical signals during propagation in the atmosphere namely scattering, scintillation etc. The Beer-Lambert theory was used to evaluate the absorption and scattering of optical signals in the atmosphere. The Kruse, Kim and Ferdinandov models were adopted to determine the scattering atmospheric attenuation for the eastern coast of Southern Africa. The Log-Normal model was employed to determine the influence of scintillation and an expression to estimate the margin required to compensate for scintillation effects was also obtained. The FSO system power scintillation index, optical beam divergence loss, link margin and link availability were discussed as well.

In chapter Four, we presented the visibility patterns, from which the atmospheric attenuation coefficients of physical layer FSO systems were determined and analyzed for the eastern coast of Southern Africa. Effects of scattering and scintillation were also examined. Power loss due to scattering and scintillation has been evaluated. Adopting the Kim model to estimate the atmospheric attenuation at 850 nm wavelength, the attenuation due to scattering was found to contribute 9.47% to the absolute atmospheric losses while the atmospheric turbulence loss contributes 90.53% to the overall power loss at a link range of 4 km. It is

also noticed that using the Ferdinandov model for a link range of 4 km at 850 nm wavelength, the attenuation due to scattering contributes 8.60% to the total power loss while the atmospheric turbulence loss contributes 91.40% to the overall power loss.

Employing the Ferdinandov model for a link range of 4 km at 950 nm wavelength, the attenuation due to scattering contributes 8.81% to the total power loss while the atmospheric turbulence loss contributes 91.19% to the overall power loss. It is also observed that using Ferdinandov model the atmospheric attenuation at 950 nm wavelength, the attenuation due to scattering contributes 7.80% to the absolute atmospheric losses while the atmospheric turbulence loss contributes 92.20% to the overall power loss for a link range of 4 km. Similarly, for a link range of 4 km at 1550 nm wavelength, the attenuation due to Mie scattering contributes 6.37% to the total power loss while the atmospheric turbulence loss contributes 93.63% to the overall power loss. The results obtained show that atmospheric turbulence or scintillation are the major contributors to the attenuation of optical signals traversing the FSO atmospheric channel.

The probability of encountering and exceeding different atmospheric fading conditions for 850 nm, 950 nm and 1550 nm wavelengths was examined. Adopting Kim model (850 nm), the probability of experiencing attenuation exceeding 0.1 dB/km is 0.972222 while the probability of encountering probability exceeding 0.5 dB/km is 0.282407 and the probability of encountering attenuation exceeding or equal to the highest recorded attenuation for the eastern coast of South Africa that is 1.2 dB/km is 0.018519. Using Ferdinandov model (850 nm), the probability of experiencing attenuation exceeding 0.1 dB/km is approximately 1 while the probability of encountering probability exceeding 0.5 dB/km is 0.25463 and the probability of encountering attenuation exceeding or equal to the highest recorded attenuation for the eastern coast of South Africa, that is, 1.2 dB/km is 0.013889.

Employing Kim model (950 nm), the probability of experiencing attenuation exceeding 0.1 dB/km is 0.967593 while the probability of encountering attenuation exceeding 0.5 dB/km is 0.069444 and the probability of encountering attenuation exceeding or equal the highest recorded attenuation for the eastern coast of South Africa, that is, 1.2 dB/km is 0.009259. Using Kim model (1550 nm), the probability of experiencing attenuation exceeding 0.1 dB/km is 0.796296 while the probability of encountering probability exceeding 0.5 dB/km is 0.037037 and the probability of encountering attenuation exceeding or equal the highest attenuation for the eastern coast of South Africa, that is, 1.2 dB/km is 0.009259.

The link margin required to compensate for losses caused by scintillation impacts was discussed. The probability of encountering and exceeding atmospheric attenuation was investigated. The FSO link budget and link availability were determined and analyzed for the eastern coast of Southern Africa. The relevance of the link budget analysis is to determine the attainable link length for various link margins as well as

receiver sensitivity. It has been shown that the attainable link distance increases with an increase in the atmospheric visibility status. The link length can be increased by increasing the propagated optical power as well. Moreover, we have investigated the availability of economical FSO systems in the eastern coast of Southern Africa by considering the atmospheric fading conditions and the optical link equation. The FSO system availability reduces with an increase in the propagation link distance.

Further investigation was carried out regarding the impacts of scintillation on optical signals by considering the lognormal model. It is observed that the fading loss from scintillation effects strongly depends on the power scintillation index. Increase in the power scintillation index causes an increase in the fading loss as well. However, the power scintillation index also increases per unit increase in the transmission link length and refractive index. The compensation margin for such atmospheric fading losses increases with a decrease in accessible FSO system bound probability. Therefore, for a highly reliable FSO system link, extra margin must be incorporated to compensate for fading losses caused by scintillation.

As an application, chapter Five examines the performance of OFDM systems mitigated by M-DPSK over free space optics channel, which shows that the OFDM system has improved in non-turbulence as compared to turbulence environment. The performance of OFDM-FSO communication system under Log-normal channel for MQAM i.e. (8-QAM, 16-QAM, 32-QAM, 64-QAM) and BPSK modulation schemes was also evaluated. The results show that there is a reduction of approximately 10^{-4} in BER for BPSK compared to 8-QAM modulation scheme used over the OFDM-FSO Log-normal channel. It is also observed that for 8-QAM modulation scheme for the same values of wavelength and SNR, BER increases with respect to increase in the Log-normal channel length. The BER versus SNR analyses carried out reveal that, in order to obtain a low BER and highly improved bandwidth, M-QAM modulation schemes should be considered while BPSK is suitable when propagating at high power for better enhanced power efficiency.

6.2 Future Work

This research work has successfully achieved the aims and objectives outlined in Chapter One. The following topics are suggested to further extend the research work reported in this dissertation. These includes Radio over FSO (RoFSO), Hybrid FSO/RF communication using channel coding, Soft-switching hybrid FSO/RF links using field-programmable gate array (FPGA), Modulation Schemes Combined with LDPC, Spatial Diversity etc.

Reference

[1] F. R. Gfeller and U. Bapst, "Wireless in-house data communication via diffuse infrared radiation," *Proceedings of the IEEE,* vol. 67, pp. 1474-1486, 1979.

[2] J. Hecht, "Beam: the race to make the laser," *Optics and photonics news,* vol. 16, pp. 24-29, 2005.

[3] F. E. Goodwin, "A review of operational laser communication systems," *Proceedings of the IEEE,* vol. 58, pp. 1746-1752, 1970.

[4] Z. Sodnik, B. Furch, and H. Lutz, "Free-space laser communication activities in Europe: SILEX and beyond," in *19th Annual Meeting of the IEEE Lasers and Electro-Optics Society (LEOS)*, 2006, pp. 78-79.

[5] P. M. Becker, A. A. Olsson, and J. R. Simpson, *Erbium-doped fiber amplifiers: fundamentals and technology*: Academic press, 1999.

[6] D. L. Begley, "Free-space laser communications: a historical perspective," in *Lasers and Electro-Optics Society, (LEOS). The 15th Annual Meeting of the IEEE*, 2002, pp. 391-392.

[7] S. Hranilovic, *Wireless optical communication systems*: Springer Science & Business Media, 2006.

[8] S. Hardy, "Free-space optics systems are finding their niches," *IEEE Journal of Lightwave,* pp. 33-36, 2005.

[9] E. J. Korevaar, I. I. Kim, and B. McArthur, "Atmospheric propagation characteristics of highest importance to commercial free space optics," in *Proceedings of SPIE*, 2003, pp. 1-12.

[10] C. Abou-Rjeily, "On the optimality of the selection transmit diversity for MIMO-FSO links with feedback," *IEEE Communications Letters,* vol. 15, pp. 641-643, 2011.

[11] M. Gregory and S. Badri-Hoeher, "Characterization of maritime RF/FSO channel," in *International Conference on Space Optical Systems and Applications (ICSOS)*, 2011, pp. 21-27.

[12] M. N. Khan and W. G. Cowley, "Signal dependent Gaussian noise model for FSO communications," in *Communications Theory Workshop (AusCTW)*, Australian, 2011, pp. 142-147.

[13] T. Plank, M. Czaputa, E. Leitgeb, S. S. Muhammad, N. Djaja, B. Hillbrand, *et al.*, "Wavelength selection on FSO-links," in *Proceedings of the 5th European Conference on Antennas and Propagation (EUCAP)*, , 2011, pp. 2508-2512.

[14] V. W. Chan, "Free-space optical communications," *Journal of Lightwave Technology,* vol. 24, pp. 4750-4762, 2006.

[15] J. J. Fernandes, P. A. Watson, and J. C. Neves, "Wireless LANs: physical properties of infra-red systems vs. MMW systems," *IEEE Communications Magazine,* vol. 32, pp. 68-73, 1994.

[16] W. O. Popoola, Z. Ghassemlooy, J. Allen, E. Leitgeb, and S. Gao, "Free-space optical communication employing subcarrier modulation and spatial diversity in atmospheric turbulence channel," *IET optoelectronics*, vol. 2, pp. 16-23, 2008.

[17] V. Sharma and N. Kumar, "Improved analysis of 2.5 Gbps-inter-satellite link (ISL) in inter-satellite optical-wireless communication (IsOWC) system," *Optics Communications*, vol. 286, pp. 99-102, 2013.

[18] M. Handura, K. Ndjavera, C. Nyirenda, and T. Olwal, "Determining the feasibility of free space optical communication in Namibia," *Optics Communications*, vol. 366, pp. 425-430, 2016.

[19] J. Mohale, M. R. Handura, T. O. Olwal, and C. N. Nyirenda, "Feasibility study of free-space optical communication for South Africa," *Optical Engineering*, vol. 55, pp. 056108-056108, 2016.

[20] S. M. Rajendrakumar and M. Karruppaswamy, "Analysis of link availability in FSO-OFDM system under various climatic conditions," *Engineering Journal*, vol. 19, pp. 85-95, 2015.

[21] W. D. Williams, M. Collins, D. M. Boroson, J. Lesh, A. Biswas, R. Orr, *et al.*, "RF and optical communications: A comparison of high data rate returns from deep space in the 2020 timeframe," 2007.

[22] J. Franz and V. K. Jain, *Optical Communications: Components and Systems: Analysis--design--optimization--application*: CRC press, 2000.

[23] M. Jeganathan, K. Wilson, and J. Lesh, "Preliminary analysis of fluctuations in the received Uplink-Beacon-Power data obtained from the GOLD experiments," 1996.

[24] H. Henniger and O. Wilfert, "An introduction to free-space optical communications," *Radioengineering*, vol. 19, p. 5, 2010.

[25] Z. Bielecki, W. Kolosowski, and J. Mikolajczyk, "Free-space optical data link using quantum cascade laser," in *PIERS Conference*, 2008, pp. 108-111.

[26] F. Liu, U. Vishkin, and S. Milner, "Bootstrapping free-space optical networks," *IEEE Journal on Selected Areas in Communications*, vol. 24, pp. 13-22, 2006.

[27] N. H. M. Noor, A. Naji, and W. Al-Khateeb, "Theoretical analysis of multiple transmitters/receivers on the performance of free space optics (FSO) link," in *IEEE International Conference on Space Science and Communication (IconSpace)*, 2011, pp. 291-295.

[28] A. Bekkali, C. B. Naila, K. Kazaura, K. Wakamori, and M. Matsumoto, "Transmission analysis of OFDM-based wireless services over turbulent radio-on-FSO links modeled by gamma–gamma distribution," *IEEE Photonics Journal*, vol. 2, pp. 510-520, 2010.

[29] H. Willebrand and B. S. Ghuman, *Free space optics: enabling optical connectivity in today's networks*: SAMS publishing, 2002.

[30] A. K. Majumdar and J. C. Ricklin, *Free-space laser communications: principles and advances* vol. 2: Springer Science & Business Media, 2010.

[31] S. Bloom, E. Korevaar, J. Schuster, and H. Willebrand, "Understanding the performance of free-space optics [Invited]," *Journal of optical Networking*, vol. 2, pp. 178-200, 2003.

[32] A. Pavelchek, R. G. Trissel, J. Plante, and S. Umbrasas, "Long-wave infrared (10-μm) free-space optical communication system," in *SPIE's 48th Annual Meeting on Optical Science and Technology*, 2004, pp. 247-252.

[33] G. Keiser, *Optical communications essentials*: McGraw-Hill, 2003.

[34] O. Bouchet, H. Sizun, C. Boisrobert, and F. De Fornel, *Free-space optics: propagation and communication* vol. 91: John Wiley & Sons, 2010.

[35] R. Gagliardi and S. Karp, "The optical communication system," ed: New York: John Wiley & Sons, Inc, 1995, pp. 1-3.

[36] X. Wu, P. Liu, and M. Matsumoto, "A study on atmospheric turbulence effects in full-optical free-space communication systems," in *6th International Conference on Wireless Communications Networking and Mobile Computing (WiCOM)*, 2010, pp. 1-5.

[37] D. Killinger, "Free space optics for laser communication through the air," *Optics and Photonics News*, vol. 13, pp. 36-42, 2002.

[38] W. K. Pratt, "Laser Communication Systems," 1969.

[39] G. R. Osche, "Optical detection theory for laser applications," *Optical Detection Theory for Laser Applications, by Gregory R. Osche, pp. 424. ISBN 0-471-22411-1. Wiley-VCH, July 2002.*, p. 424, 2002.

[40] S. Karp, R. M. Gagliardi, S. E. Moran, and L. B. Stotts, *Optical channels: fibers, clouds, water, and the atmosphere*: Springer Science & Business Media, 2013.

[41] S. Betti, G. De Marchis, and E. Iannone, *Coherent optical communications systems*: Wiley-Interscience, 1995.

[42] D. Bohren, "Huffman," *Absorption and scattering of light by small particles", John Willey & Sons, New York*, 1983.

[43] M. S. Islam, A. Mohammad, and S. A. Al-Gailani, "Characteristics of free space optics communication link in an unusual haze," *Indian Journal of Pure and Applied Physics*, vol. 54, pp. 46-50, 2016.

[44] E. Leitgeb, M. Gebhart, and U. Birnbacher, "Optical networks, last mile access and applications," *Journal of Optical and Fiber Communications Reports*, vol. 2, pp. 56-85, 2005.

[45] M. Ijaz, "Experimental Characterisation and Modelling of Atmospheric Fog and Turbulence in FSO," Northumbria University, 2013.

[46] A. Alkholidi and K. Altowij, *Effect of clear atmospheric turbulence on quality of free space optical communications in Western Asia*: INTECH Open Access Publisher, 2012.

[47] M. Naboulsi, H. Sizun, and F. Fornel, "Propagation of optical and infrared waves in the atmosphere," *Proceedings of the union radio scientifique internationale*, 2005.

[48] T. H. Carbonneau and D. R. Wisely, "Opportunities and challenges for optical wireless: the competitive advantage of free space telecommunications links in today's crowded marketplace," in *Voice, Video, and Data Communications*, 1998, pp. 119-128.

[49] A. Ramezani, M. Noroozi, and M. Aghababaee, "Analyzing free space optical communication performance," *Int. J. Eng. Adv. Technol*, vol. 4, pp. 46-51, 2014.

[50] C. B. Naila, A. Bekkali, K. Wakamori, and M. Matsumoto, "Performance analysis of CDMA-based wireless services transmission over a turbulent RF-on-FSO channel," *Journal of Optical Communications and Networking*, vol. 3, pp. 475-486, 2011.

[51] L. C. Andrews, R. L. Phillips, and C. Y. Hopen, *Laser beam scintillation with applications* vol. 99: SPIE press, 2001.

[52] A. Prokes, "Atmospheric effects on availability of free space optics systems," *Optical Engineering*, vol. 48, pp. 1-10, 2009.

[53] N. S. Singh and G. Singh, "Performance Evaluation of Log-normal And Negative Exponential Channel Modeling Using Various Modulation Techniques in OFDM-FSO Communication," *International Journal of Computers & Technology*, vol. 4, pp. 639-647, 2013.

[54] J. Armstrong, "OFDM for optical communications," *Journal of lightwave technology*, vol. 27, pp. 189-204, 2009.

[55] M. Selvi and K. Murugesan, "Performance of OFDM based FSO communication systems using M-ary PSK modulation," *International Journal of Computer Applications*, vol. 49, 2012.

[56] K. Tsukamoto, A. Hashimoto, Y. Aburakawa, and M. Matsumoto, "The case for free space," *IEEE microwave magazine*, vol. 10, 2009.

[57] S. M. Rajendrakumar, M. Karruppaswamy, P. Praserthdam, E. Editor, E. Intakan, E. Office, *et al.*, "Analysis of link availability in FSO-OFDM system under various climatic conditions," *Engineering Journal*, vol. 19, 2015.

[58] Z. Ghassemlooy, W. Popoola, and S. Rajbhandari, *Optical wireless communications*: CRC Press Boca Raton, FL, 2012.

[59] S. Popescu, G. Budura, and A. Gontean, "Review of PSK and QAM—Digital modulation techniques on FPGA," in *International Joint Conference on Computational Cybernetics and Technical Informatics (ICCC-CONTI)*, 2010, pp. 327-332.